PRMT1 Is Critical for the Transcriptional Activity and the Stability of the Progesterone Receptor.

Lucie Malbeteau, Coralie Poulard, Cécile Languilaire, Ivan Mikaelian, Frederic Flamant, Muriel Le Romancer, Laura Corbo

iScience

CellPress
OPEN ACCESS

Article

PRMT1 Is Critical for the Transcriptional Activity and the Stability of the Progesterone Receptor

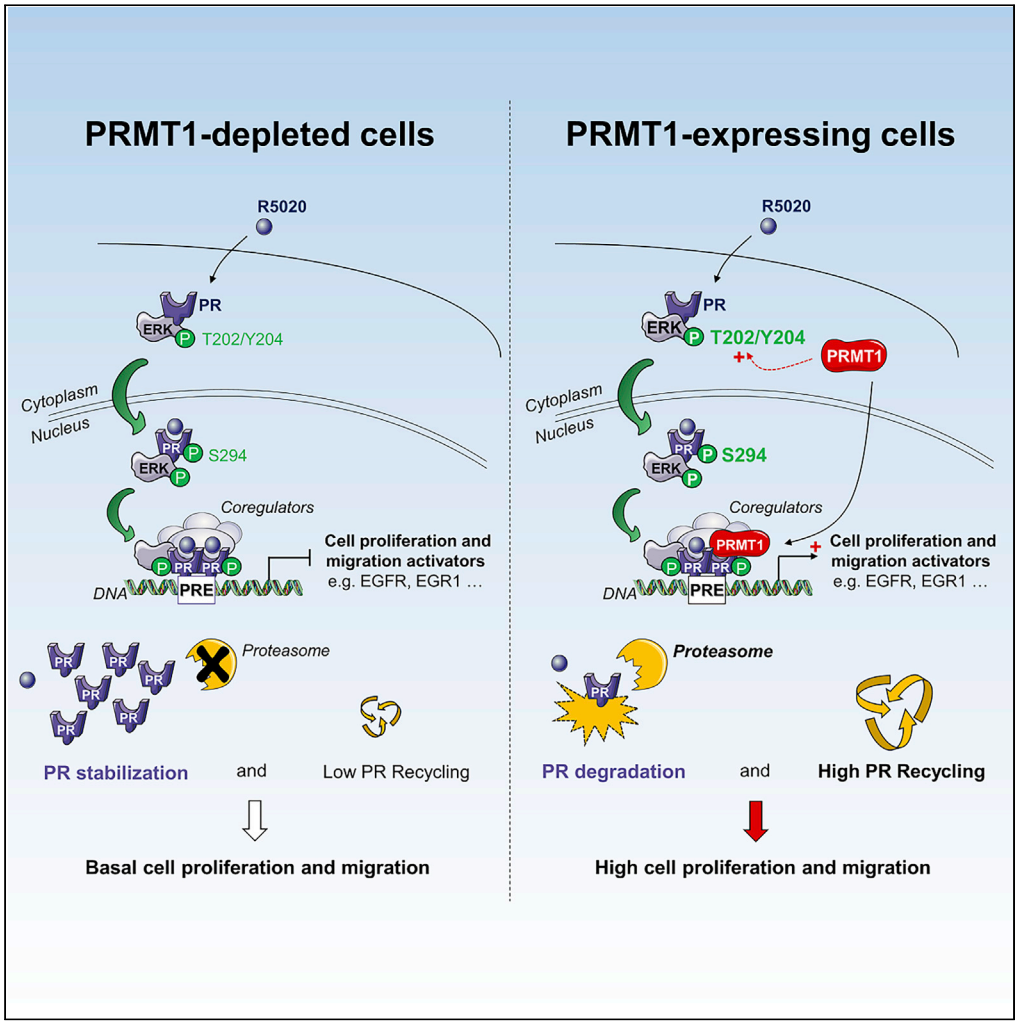

Lucie Malbeteau, Coralie Poulard, Cécile Languilaire, Ivan Mikaelian, Frédéric Flamant, Muriel Le Romancer, Laura Corbo

muriel.leromancer@lyon.unicancer.fr (M.L.R.)
laura.corbo@lyon.unicancer.fr (L.C.)

HIGHLIGHTS

The progesterone receptor (PR) is methylated by PRMT1 upon progestin treatment

PRMT1-dependent methylation controls the stability of PR

PRMT1 activates genes involved in the regulation of cell migration and invasion

PRMT1 expression influences the survival of patients with PR-positive breast cancer

Malbeteau et al., iScience *23*, 101236
June 26, 2020
https://doi.org/10.1016/j.isci.2020.101236

iScience

CellPress
OPEN ACCESS

Article

PRMT1 Is Critical for the Transcriptional Activity and the Stability of the Progesterone Receptor

Lucie Malbeteau,[1,2] Coralie Poulard,[1,2] Cécile Languilaire,[1,2] Ivan Mikaelian,[1,2] Frédéric Flamant,[1,3] Muriel Le Romancer,[1,2,*] and Laura Corbo[1,2,4,*]

SUMMARY

The progesterone receptor (PR) is an inducible transcription factor that plays critical roles in female reproductive processes and in several aspects of breast cancer tumorigenesis. Our report describes the type I protein arginine methyltransferase 1 (PRMT1) as a cofactor controlling progesterone pathway, through the direct methylation of PR. Mechanistic assays in breast cancer cells indicate that PRMT1 methylates PR at the arginine 637 and reduces the stability of the receptor, thereby accelerating its recycling and finally its transcriptional activity. Depletion of PRMT1 decreases the expression of a subset of progesterone-inducible genes, controlling breast cancer cells proliferation and migration. Consistently, Kaplan-Meier analysis revealed that low expression of PRMT1 predicts a longer survival among the subgroup with high PR. Our study highlights PR methylation as a molecular switch adapting the transcription requirement of breast cells during tumorigenesis.

INTRODUCTION

The progesterone receptor (PR) is a member of the nuclear hormone receptor family of ligand-dependent transcription factors (Mangelsdorf et al., 1995). Acting through its cognate steroid hormone progesterone, PR regulates the expression of gene networks to control development, differentiation, and proliferation of female reproductive tissues during the ovarian cycle and pregnancy (Brisken and O'Malley, 2010). Furthermore, numerous studies have established that PR is an important regulator of several aspects of breast cancer tumorigenesis and progression, including cell migration and invasiveness (Grimm et al., 2016; Knutson and Lange, 2014). Two major isoforms of PR exist across species, the longer PR-B and the shorter PR-A, which differ in promoter usage (Kastner et al., 1990). They are differentially expressed and exhibit distinct functions *in vivo*; PR-A is more responsible for progesterone actions in uterus and ovary, whereas PR-B is required for mammary gland development (Mulac-Jericevic et al., 2003), mediating the proliferative actions of progestins (Boonyaratanakornkit et al., 2001; Faivre and Lange, 2007).

PR activity is regulated by extensive post-translational modifications (PTMs) that include phosphorylation, acetylation, ubiquitination, SUMOylation, and methylation (reviewed in Abdel-Hafiz and Horwitz, 2014; Knutson and Lange, 2014). These modifications affect PR hormone sensitivity, subcellular localization, protein stability, or interactions with cofactors. For example, progesterone stimulation induces MAPK-dependent phosphorylation of its receptor on the serine 294 (Ser-294 or S294), a key modification essential for the activation and the enhancement of PR transcriptional activity. Paradoxically, this event is also a signal for the ligand-dependent degradation of the receptor, essential for its regulated transcriptional functions (Lange et al., 2000; Shen et al., 2001).

The molecular mechanisms underlying PR-dependent transcription have been extensively studied, both in the absence of, and upon exposure to progesterone (Beato and Vicent, 2012; Jacobsen and Horwitz, 2012). These studies converge to a simplified model of gene expression induced by progestins: before hormonal treatment, PR binds genomic sites within a repressive complex maintaining these genes silenced prior to hormone treatment (Vicent et al., 2013). Progestin stimulation leads to the activation of cytoplasmic downstream kinase cascades, including ERK1/2, and finally to PR phosphorylation, especially on Ser-294 (Migliaccio et al., 1998). This active phosphorylated form of PR, associated with kinases, induces the

[1]Université Lyon 1, Lyon F-69000, France

[2]Inserm U1052 CNRS UMR 5286, Cancer Research Center of Lyon, Centre Léon Bérard, Lyon F-69008, France

[3]Institut de Génomique Fonctionnelle de Lyon, INRA USC 1370, CNRS UMR 5242, Ecole Normale Supérieure de Lyon, Lyon Cedex 07, France

[4]Lead Contact

*Correspondence: muriel.leromancer@lyon.unicancer.fr (M.L.R.), laura.corbo@lyon.unicancer.fr (L.C.)

https://doi.org/10.1016/j.isci.2020.101236

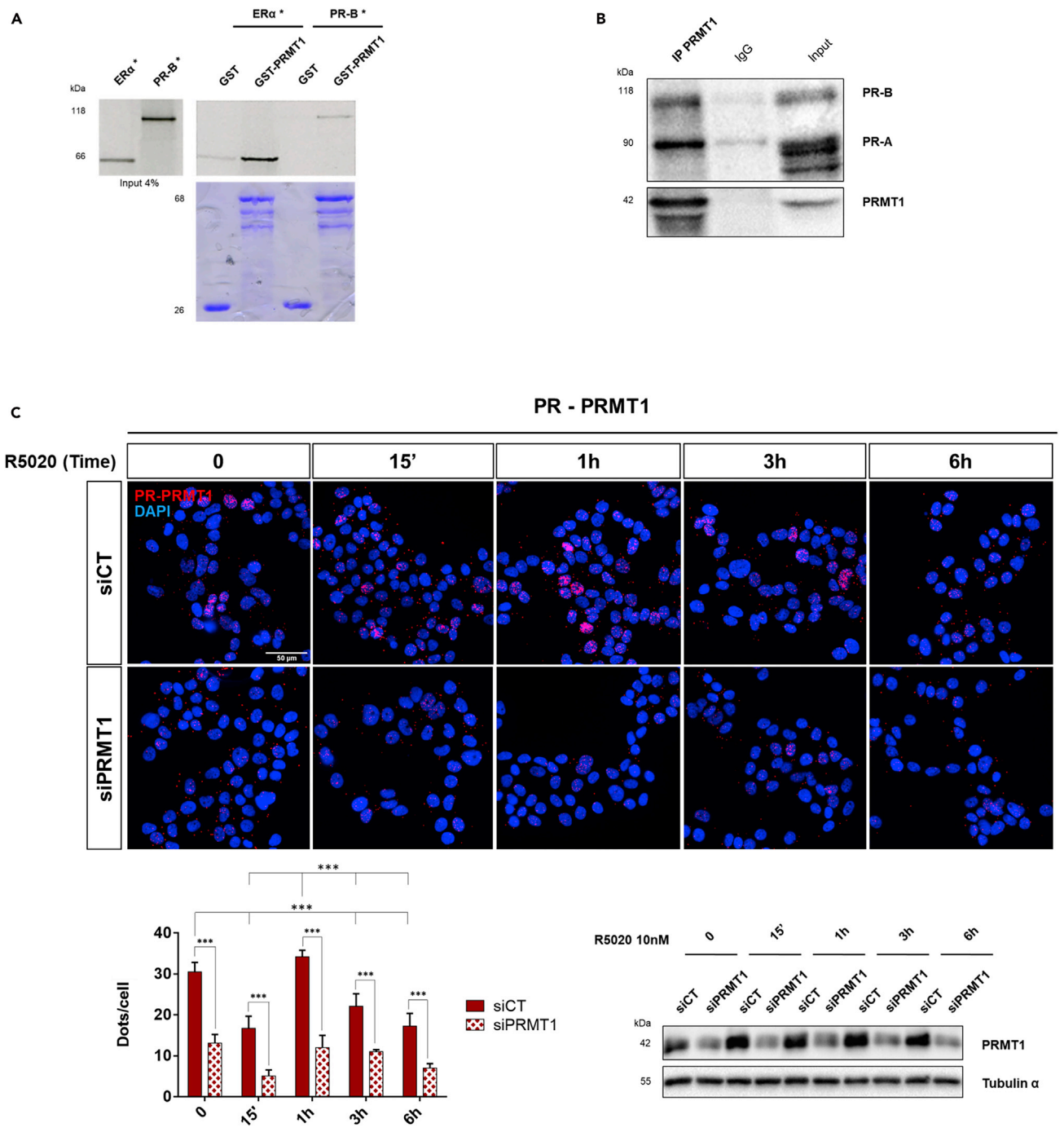

Figure 1. PRMT1 Interacts with PR in R5020-Stimulated T47D Breast Cancer Cells

(A) GST pull-down experiment: ^{35}S-labeled *in vitro* translated PR-B, and ERα used as a positive control, were incubated with GST and GST-PRMT1 bound to glutathione Sepharose beads. The eluted proteins were analyzed by SDS-PAGE and visualized by autoradiography. Autoradiograph (upper) and Coomassie staining (lower) are shown.

(B) Whole-cell extracts (WCE) of T47D were subjected to immunoprecipitation (IP) using anti-PRMT1 antibody, or control IgG, and immunoblotted (IB) with anti-PR antibody.

(C) Proximity ligation assay (PLA) was used to detect the endogenous interaction between PRMT1 and PR in T47D cells, using anti-PR and anti-PRMT1 antibodies. T47D cells were transfected with control siRNA (siCT) or with anti-PRMT1 siRNAs (siPRMT1) and were cultured in medium deprived of steroids for

Figure 1. *Continued*
48 h, prior to the addition of R5020 (10 nM) for the indicated times. The nuclei were counterstained with DAPI (blue) (Obj: X60). The interactions are represented by red dots. Lower panel (left) shows the quantification of the number of signals per cell, as described in the Transparent Methods section. The mean ± SD of one experiment representative of three experiments is shown. The p value was determined using the Student's t test: *** indicates $p \leq 0.001$. The efficacy of PRMT1 siRNA treatment is analyzed by IB and shown in the lower panel (right).

recruitment of histone-modifying enzymes. This is followed by a local chromatin remodeling and the assembly of the transcription initiation complex on progestin-regulated genes (Beato and Vicent, 2012).

Protein arginine methyltransferases (PRMTs) are one such class of histone-modifying enzymes that regulate transcription. Two primary transcriptional coactivators in this family are PRMT1 and CARM1 (Coactivator Associated arginine (R) Methyltransferase 1), recruited as coregulators on promoters of genes targeted by nuclear receptors (Koh et al., 2001; Wang et al., 2001). PRMT1 is the predominant asymmetric arginine methyltransferase in humans and functions as a general transcriptional coactivator, by depositing dimethylarginines on histone 4 (H4R3me2as). However, PRMT1 also dimethylates a large variety of non-histone substrates, regulating many cellular processes required for tissue homeostasis, including RNA processing, transcriptional regulation, signal transduction, DNA repair, and protein-protein interactions (Bedford and Clarke, 2009; Blanc and Richard, 2017). Moreover, aberrant expression of PRMT1 has been reported in several malignancies, including breast cancer, although how PRMT1 contributes to oncogenesis remains largely elusive (Poulard et al., 2016; Yang and Bedford, 2013). We have previously shown that PRMT1 regulates the function of the estrogen receptor ERα through the methylation of the arginine 260, leading to the formation of a cytoplasmic signaling complex activated in aggressive human breast tumors (Le Romancer et al., 2008; Poulard et al., 2012).

We herein highlight the involvement of PRMT1 in breast tumorigenesis through, at least in part, the direct methylation of the progesterone receptor at the arginine 637. PRMT1 interacts with and regulates PR functions, acting as an essential actor of progesterone signaling in breast cancer cells. Our results indicate that PRMT1 and arginine methylation control PR stability, leading to the modulation of its transcriptional activity. PRMT1 allows the activation of a subset of genes controlling proliferation and survival of breast cancer cells and its expression clearly influences the clinical outcome of breast cancer according to PR expression.

RESULTS

PRMT1 Interacts with the Progesterone Receptor in T47D Cancer Cells

To test whether PR might be regulated by arginine methylation, we initially examined a physical association between PR and PRMT1 *in vitro* and in T47D mammary carcinoma cells, which contain constitutive high levels of PR (Smith et al., 2017). Using a GST-binding assay, we showed the direct binding between PR and PRMT1 (Figure 1A). When T47D cell extracts were immunoprecipitated using an anti-PRMT1 antibody, coimmunoprecipitation (coIP) of both PR isoforms were observed (Figure 1B). Given the functional specificity of PR-B in breast (Boonyaratanakornkit et al., 2001; Faivre and Lange, 2007), we focused our study essentially on this isoform (called PR). As PR is a ligand-regulated nuclear transcription factor, we investigated whether the PR-PRMT1 interaction was hormone dependent and in which cellular compartment it occurred. For that, T47D cells were starved in medium deprived of steroids for 48 h (time 0) prior to the treatment for the indicated times with R5020 (also known as Promegestone), a synthetic agonist of progesterone used in scientific studies because of its stability (Read et al., 1988; Vignon et al., 1983). To localize and quantify these interactions more precisely, we used the *in situ* proximity ligation assay (PLA) (Poulard et al., 2014; Söderberg et al., 2006). The presence of red dots indicates interactions between endogenous PR and PRMT1 that occurred mainly in the nucleus and varied during the course of R5020 induction (Figure 1C). The graph representing the counting of dots per 100 cells indicated a high number of interactions between the two proteins in the absence of hormonal induction (Figure 1C, lower left panel). Notably, 15 min of R5020 treatment engendered a significant reduction in the signal abundancy, reflecting the dissociation of the PR-PRMT1 complex; then a second interaction peak was detected after 1 h of treatment (Figure 1C, lower left panel). A strong decrease in dot numbers was observed when the expression of PRMT1 or PR was knocked down using a pool of siRNAs, compared with mock T47D cells transfected with scramble siRNA (siCT) (Figure 1C, lower right panel and Figures S1A–S1C), validating the specificity of the PR-PRMT1 interaction, which is nuclear, dynamic, and progesterone-regulated.

PRMT1 Methylates PR at a Conserved Site *In Vitro* and in Cells

We then investigated whether PR was methylated in T47D cells using two complementary approaches. First, extracts from V5-tagged PR T47D-transfected cells stimulated with R5020 for 1 h were

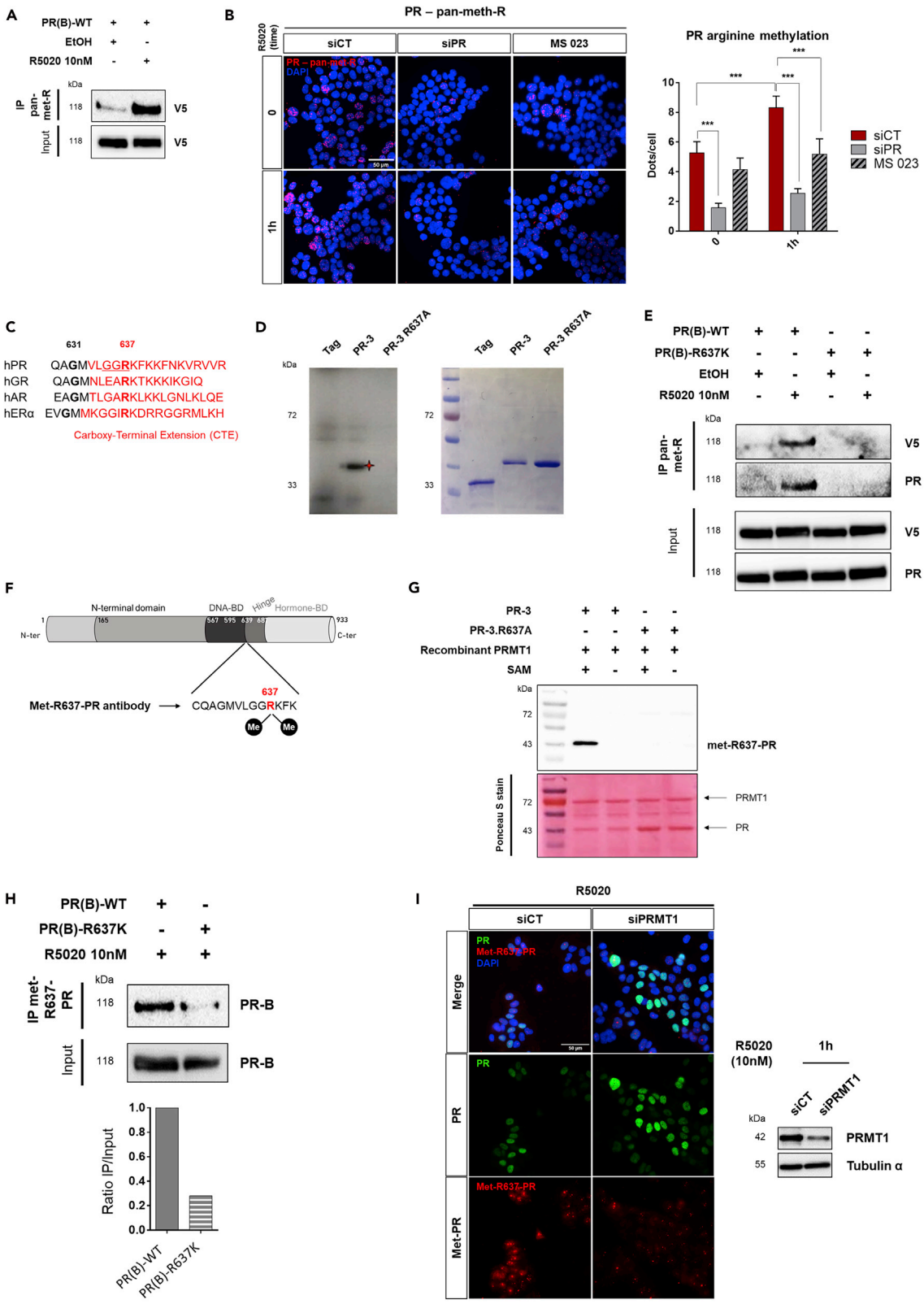
A
PR(B)-WT + +
EtOH + -
R5020 10nM - +
kDa
IP pan-met-R
118
V5
Input
118
V5
B
PR – pan-meth-R
R5020 (time)
siCT
siPR
MS 023
0
1h
PR – pan-meth-R
DAPI
50 µm
PR arginine methylation
Dots/cell
siCT
siPR
MS 023
***
C
631 637
hPR QAGMVLGGRKFKKFNKVRVVR
hGR QAGMNLEARKTKKKIKGIQ
hAR EAGMTLGARKLKKLGNLKLQE
hERα EVGMMKGGIRKDRRGGRMLKH
Carboxy-Terminal Extension (CTE)
D
Tag
PR-3
PR-3 R637A
kDa
72
33
E
PR(B)-WT + + - -
PR(B)-R637K - - + +
EtOH + - + -
R5020 10nM - + - +
kDa
IP pan-met-R
118
V5
118
PR
Input
118
V5
118
PR
F
N-terminal domain
DNA-BD
Hinge
Hormone-BD
1
165
567 595 639 687
933
N-ter
C-ter
Met-R637-PR antibody
637
CQAGMVLGGRKFK
Me
Me
G
PR-3 + + - -
PR-3.R637A - - + +
Recombinant PRMT1 + + + +
SAM + - + -
kDa
72
43
met-R637-PR
Ponceau S stain
72
43
PRMT1
PR
H
PR(B)-WT + -
PR(B)-R637K - +
R5020 10nM + +
kDa
IP met-R637-PR
118
PR-B
Input
118
PR-B
Ratio IP/Input
1.0
0.8
0.6
0.4
0.2
0.0
PR(B)-WT
PR(B)-R637K
I
R5020
siCT
siPRMT1
Merge
PR
Met-R637-PR
DAPI
PR
PR
Met-R637-PR
Met-PR
R5020 (10nM)
1h
siCT
siPRMT1
kDa
42
PRMT1
55
Tubulin α

Figure 2. PRMT1 Methylates PR at Arginine 637 under Progesterone Treatment

(A) WCE from T47D, transfected with V5-tagged wild-type PR(B) (PR(B)-WT) plasmid and treated for 1h with R5020 were collected and immunoprecipitated (IP) with anti-pan-meth-R, or anti-immunoglobulin G (IgG), followed by IB using V5 antibody.

(B) PLA used to detect endogenous PR asymmetrically dimethylated on arginine sites in T47D cells, using anti-PR and anti-pan-meth-R antibodies. Cells were transfected with control siRNA (siCT) or with anti-PR siRNAs (siPR) or treated with MS 023 inhibitor (60 nM), then treated with R5020 (1 h) or vehicle ethanol (0). The analysis and the quantification of PLA experiments were performed as in Figure 1C.

(C) Alignment of the carboxy-terminal extensions of steroid receptors with conserved arginine (R) sequence in a similar position.

(D) An *in vitro* methylation assay using recombinant GST-PR-3 fragments, wild-type (WT) or mutated at R637 (PR-3 R637A) incubated with recombinant GST-PRMT1, in the presence of [methyl-3H] SAM. Reaction products were analyzed by SDS-PAGE followed by fluorography. The migration and the quality of recombinant GST-PR fragments were verified by a Coomassie-stained SDS-PAGE gel, shown in the right panel.

(E) WCE from T47D cells transfected with V5-tagged PR-WT or -R637K plasmids and treated for 1 h with R5020, were used for IP with pan-meth-R antibody and analyzed by IB using V5 and PR antibodies.

(F) Polyclonal anti-met-R637-PR antibody was generated using the annotated peptide encompassing asymmetrically dimethylated-R637 as antigen.

(G) *In vitro* methylation assay, using GST-PRMT1 and cold SAM, showed that met-R637-PR antibody only detected wild-type GST-PR-3. The membrane was colored by Ponceau S stain and is shown in the lower panel.

(H) Cos7 cells were transfected with V5-tagged PR-WT or -R637K encoding plasmids and treated for 1 h with R5020. WCE were immunoprecipitated with the met-R637-PR antibody followed by IB with anti-PR antibody. Quantification of immunoprecipitated methylated PR was determined relative to the input using ChemiDoc MP (Bio-Rad), for one experiment representative of three independent experiments.

(I) Immunofluorescence assay was performed using T47D cells, transfected with siCT or siPRMT1 and stimulated with R5020 (10 nM, 1 h) using the met-R637-PR and anti-PR antibodies. The nuclei were counterstained with DAPI (blue) (Obj: X40). PRMT1 expression was verified by IB (right).

immunoprecipitated using a pan-methylarginine antibody against asymmetric dimethyl-arginine (adme-R, note pan-meth-R), the type of methylation that marks PRMT1 deposits, and probed with anti-V5 antibody. We found that PR was dimethylated in cells mostly after hormonal treatment (Figure 2A). To confirm, we used PLA analysis with anti-PR and anti-pan-meth-R antibodies to detect asymmetrically dimethylated forms of PR (Poulard et al., 2019). We observed a nuclear signal, increased after R5020 stimulation in T47D cells (Figure 2B). The methylation signal was significantly decreased after PR knockdown and in presence of MS 023, a selective inhibitor of type I PRMT-dependent methylation (Eram et al., 2016), validating the signal specificity (Figure 2B). The effect and the optimal concentration of this inhibitor on PRMT1 activity was validated on H4R3 dimethylation, a known target of PRMT1, by immunofluorescence (IF) and immunoblot (IB), and the concentration of 60 nM was selected for our experiments (Figures S2A and S2B). Collectively, these data identify PR as a potential novel substrate for PRMT1.

Then, we performed *in vitro* methylation assays using the purified GST-tagged PR fragments illustrated in Figure S2C, incubated with recombinant GST-PRMT1 (Figure S2D), in order to identify the region(s) of PR that are methylated by PRMT1. Among the various functional domains of PR, PRMT1 specifically dimethylated only the fragments 3 and 4, spanning in the DNA-binding domain (DBD) and the hinge region, suggesting that arginine methylation by PRMT1 mainly occurs in the 587–687 amino acids region (Figures S2C and S2D). Of interest, this region encompasses the C-terminal extension (CTE) region, previously described as a dynamic region involved in DNA binding, nuclear localization, interaction with coregulators of the receptor (Daniel et al., 2010; Hill et al., 2009), as well as a hot spot for PTMs, including the PRMT1-dependent methylation of ERα (Le Romancer et al., 2008). Sequence alignment of steroid receptor CTEs showed a conserved position for the arginine 637 (Arg-637 or R637) residue, within a GGR motif that PRMT1 preferentially targets, localized in the PR-3 fragment (Figure 2C). To assess whether this motif was a direct target for the enzyme, we mutated the R637 to alanine residue (R637A) into the GST-PR3 fragment, leading to a complete loss of the methylation signal *in vitro* (Figure 2D).

Further analyses were conducted in the context of full-length PR in T47D cells. For *in vivo* studies, the R637 was substituted to lysine (R637K) in order to preserve its positive charge. The wild-type (PR(B)-WT) and mutated versions (PR(B)-R637K) of V5-tagged PR were expressed into T47D cells, immunoprecipitated with the pan-meth-R antibody, and revealed with anti-V5 antibody. Figure 2E shows that PR methylation was induced after hormonal stimulation. The R637K mutation strongly impaired PR modification, confirming this residue as the principal site of arginine methylation on PR.

We therefore focused on PR-R637 methylation and analyzed its role in progesterone signaling. We generated an antibody recognizing the asymmetric dimethylation of PR on R637 (R637me2(as), named anti-met-R637-PR). As an epitope, we used a branched peptide that contains the asymmetric dimethylated arginine (Figure 2F). The functionality and specificity of the antibody were established using several approaches *in vitro* and in cells. By western blot analysis, the anti-met-R637-PR specifically detected only the *in vitro*

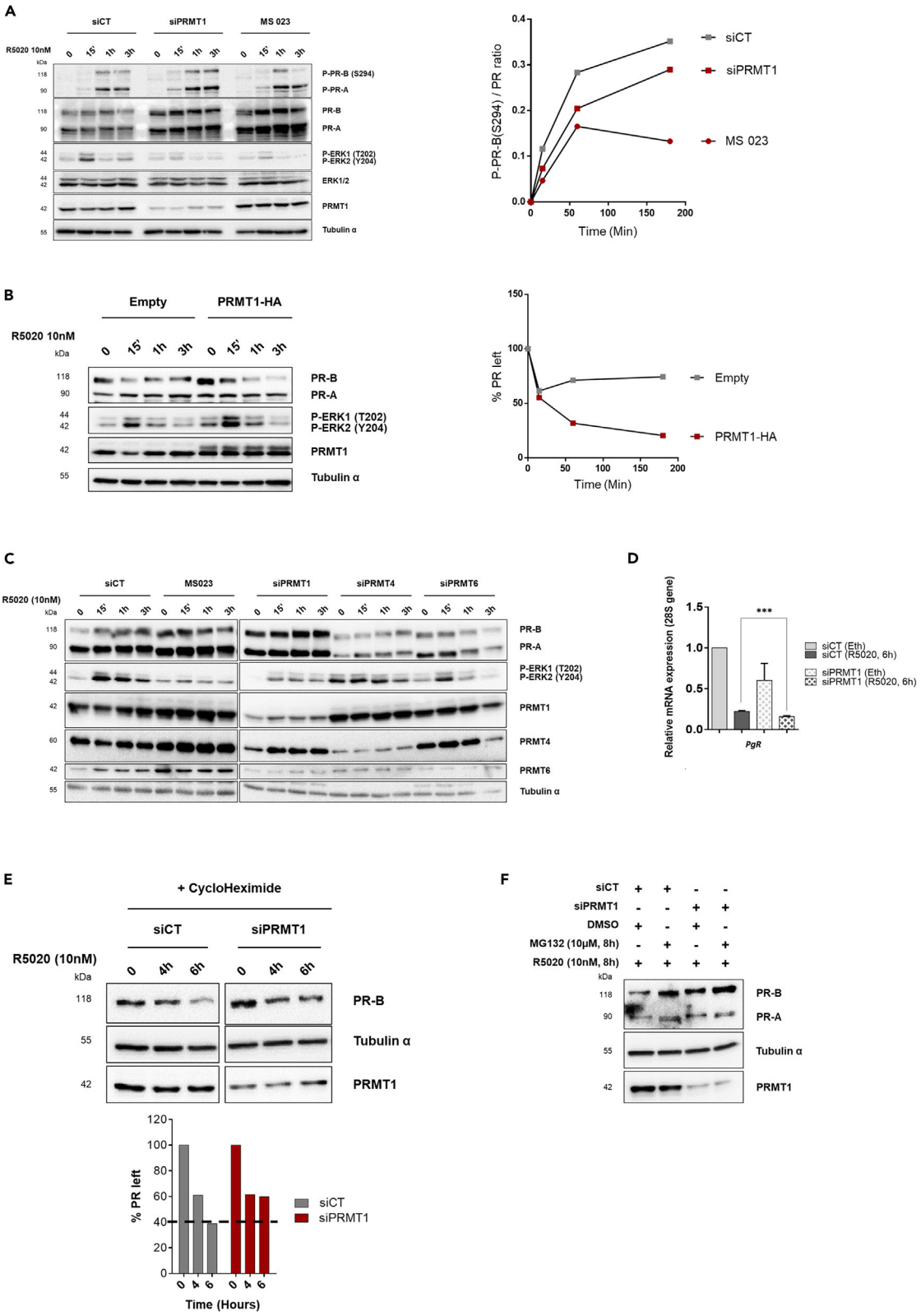
A
siCT
siPRMT1
MS 023
R5020 10nM
0
15'
1h
3h
kDa
P-PR-B (S294)
P-PR-A
PR-B
PR-A
P-ERK1 (T202)
P-ERK2 (Y204)
ERK1/2
PRMT1
Tubulin α
P-PR-B(S294) / PR ratio
Time (Min)
siCT
siPRMT1
MS 023
B
Empty
PRMT1-HA
% PR left
C
MS023
siPRMT4
siPRMT6
D
Relative mRNA expression (28S gene)
***
PgR
siCT (Eth)
siCT (R5020, 6h)
siPRMT1 (Eth)
siPRMT1 (R5020, 6h)
E
+ CycloHeximide
4h
6h
Time (Hours)
F
DMSO
MG132 (10μM, 8h)
R5020 (10nM, 8h)

Figure 3. PRMT1 Regulates Progesterone Signaling, Inhibiting the Phosphorylation and the Proteasomal Degradation of PR

(A) WB of T47D cells silenced for PRMT1 (siPRMT1) or transfected with siRNA control (siCT), or treated with MS 023 (60 nM), and stimulated with R5020 (10 nM) for the indicated times (left). Quantification of phospho-PR [P-PR-B (S294)] band intensity relative to total PR-B was measured by ChemiDoc MP (Biorad). The ratio was calculated for each time point and is shown graphically (right).

(B) WB of T47D cells transfected with HA-PRMT1 or empty-HA plasmids and treated with R5020 (left). Quantification of PR-B band intensity for each time was measured by ChemiDoc software (Biorad) (right).

(C) WCE from T47D cells, depleted for PRMT1, PRMT4, or PRMT6 by specific siRNA pool or treated with 60 nM of MS 023 inhibitor, then stimulated with R5020, were analyzed by IB.

(D) RT-qPCR of PR mRNA from T47D cells, transfected with siPRMT1 or with siCT and treated with R5020 (10 nM) for 6 h. The mean ± SEM of at least three experiments is shown. Mean values were normalized against the expression of 28S ribosomal mRNA as reference. The p value was calculated using a paired t test: *** indicates $p \leq 0.001$.

(E) Half-life study of endogenous PR-B protein. Lysates from T47D cells depleted or not for PRMT1 as in (A) were collected at the indicated time points after addition of cycloheximide and subjected to IB (top). The amount of PR-B was quantified by densitometry using the ChemiDoc software (Biorad).

(F) T47D cells were transfected with siCT or with siPRMT1 and treated with the proteasome inhibitor MG132 (10 μM) for 8 h or vehicle DMSO, before R5020 treatment. WCE were analyzed by IB. IB quantifications were done for one experiment, representative of three independent ones.

methylated WT PR-3 fragment and not the R637A mutant (Figure 2G). Dot blot experiments confirmed this specificity, as the antibody detected only the asymmetric dimethylated R637 peptide (Figure S2E). V5-tagged-wild-type (PR(B)-WT) or -mutated forms of PR (PR(B)-R637K) were expressed in PR-negative Cos7 cells, immunoprecipitated with the anti-met-R637-PR antibody and then probed with anti-PR antibody. Figure 2H shows that wild-type PR was methylated after hormonal treatment, whereas the methylation signal was strongly reduced in PR(B)-R637K protein. Additionally, we used this antibody to explore the subcellular localization of methylated PR at the endogenous level. Immunofluorescence experiments confirmed the methylation of endogenous PR in the nucleus, upon hormonal treatment, as observed with PLA (Figures 2I and 2B). Importantly, PRMT1-knockdown cells, as well as treated with the MS 023 inhibitor, displayed a marked decrease in nuclear methyl-PR signals (Figures 2I and S2F). Taken together, these data indicate that hormonal-activated PR is specifically methylated by PRMT1 on R637 in breast cancer cells.

PRMT1 Influences Progesterone Signaling by Regulating PR Stability

To pinpoint the role of PRMT1-dependant methylation in progesterone signaling, starved T47D cells were treated with 10 nM of R5020, inducing the rapid and transient activation of ERK 1 and 2 kinase activities, by phosphorylation of threonine 202 (T202) and tyrosine 204 (Y204), respectively (Hagan et al., 2012). The activation of these kinases led to the phosphorylation of PR on serine 294 (S294), described as the transcriptionally "primed" form of the receptor (Figure 3A, left panel) (Faivre et al., 2008; Lange et al., 2000). Of note, PRMT1-knockdown cells, as well as cells treated with the MS 023 inhibitor, displayed an impaired ERK activation following progestin treatment and an increase of PR protein level (Figure 3A, left panel). The quantification of the S294 phosphorylation signal, normalized to the signal of total PR, indicated that the inhibition of PRMT1 and its activity decreased the agonist-induced S294 phosphorylation of PR (Figure 3A, right panel). Supporting these data, over-expression of PRMT1 resulted in an increased activation of ERK and a decreased amount of PR following progestin treatment (Figure 3B). In contrast, the silencing of PRMT4 or PRMT6, both members of class I PRMT, did not increase the level of PR or impaired ERK activation after R5020 treatment, confirming a specific role of PRMT1 on PR signaling (Figure 3C). As the increased PR protein level was not associated with an increased synthesis of its mRNA (Figure 3D), we primarily focused on elucidating how PRMT1 controls the stability of the PR protein. Importantly, in chase experiments with the protein synthesis inhibitor cycloheximide, the half-life of endogenous PR protein was extended after depleting PRMT1 (Figure 3E), suggesting that PRMT1 controls PR expression largely through a post-translational mechanism. In agreement with these data, proteasome inhibitor MG132 treatment increased the R5020-activated PR levels, both in control and in PRMT1-depleted cells (Figure 3F), confirming the proteasome machinery involvement in the PR degradation, as described for the majority of nuclear receptors (Helzer et al., 2015).

Collectively, these results suggest that PRMT1 and its enzymatic activity are required for the progestin-dependent degradation of the receptor. The effects of PRMT1 knockdown are reminiscent of the phenomena reporting that, inhibitors of MAPK or of the 26S proteasome, blocked PR turnover, leading to a decrease of its transcriptional activity (Lange et al., 2000).

PRMT1 Acts as a PR Coregulator in Breast Cancer Cells

Because PRMT1 has been previously described as a coactivator of several nuclear receptors (Koh et al., 2001; Stallcup et al., 2000), we addressed its role in regulating the transcriptional activity of PR. A

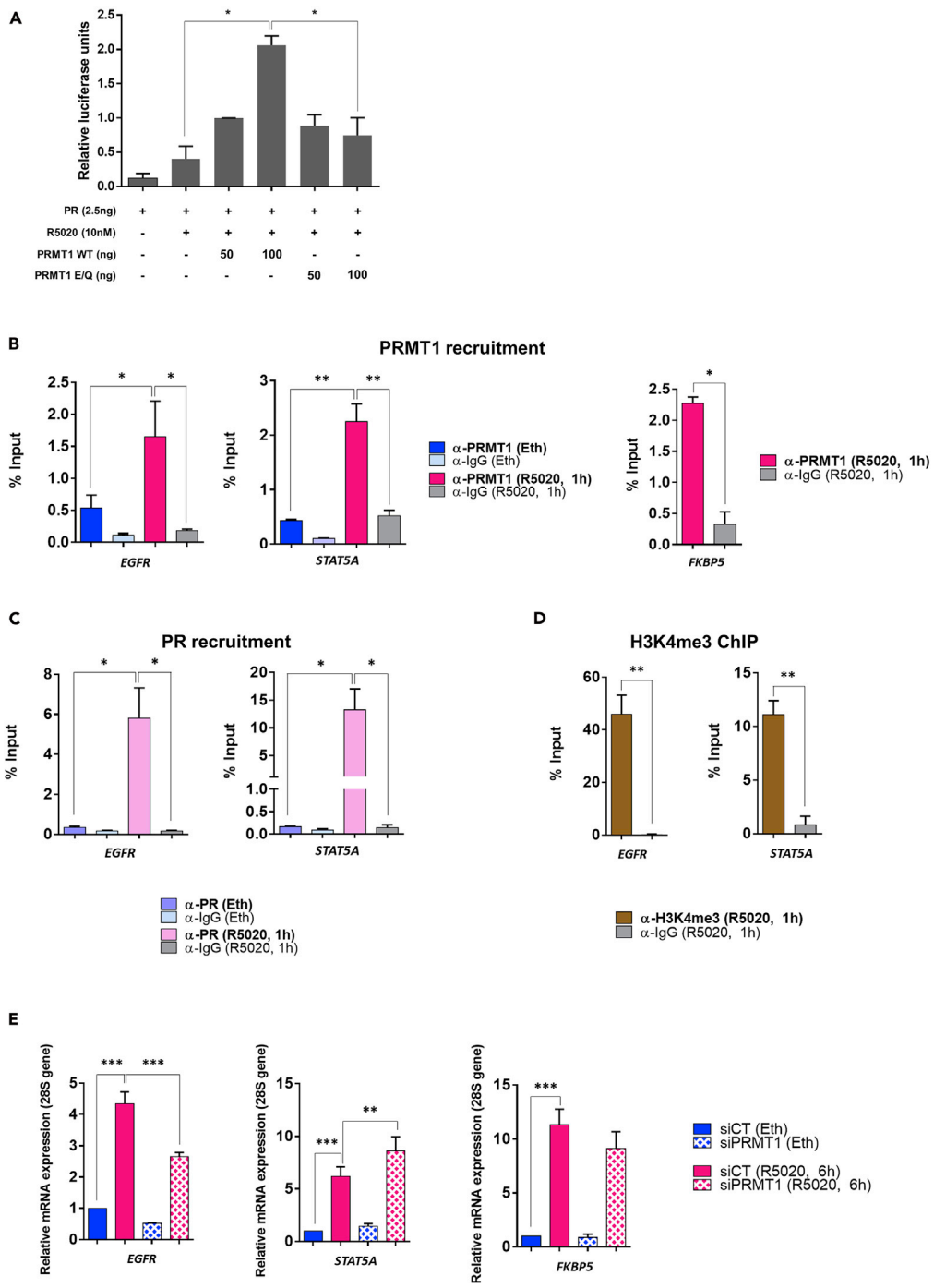

Figure 4. PRMT1 Acts as a PR Coregulator in Breast Cancer Cells

(A) HeLa cells were transfected with MMTV-LUC reporter plasmid and expression vectors encoding PR and wild-type or catalytic-mutant PRMT1 (E/Q). After R5020 treatment (10 nM), cell extracts were tested for luciferase activity using the Promega luciferase assay kit. The p value was determined using the Student's t test: * indicates $p \leq 0.05$.

(B–D) Starved T47D cells untreated (Eth) or treated with R5020 (10 nM for 1 h) were collected and subjected to chromatin immunoprecipitation (ChIP) with (B) anti-PRMT1, (C) anti-PR, and (D) anti-H3K4met3 antibodies, or control IgG. The precipitated DNA fragments were used for qPCR analysis using specific primers with respect to the input DNA and normalized to a reference locus (human chromosome 1 gene). The p value was calculated using a paired t test: * indicates $p \leq 0.05$ and **$p \leq 0.01$.

Figure 4. *Continued*

(E) T47D cells, transfected with siCT or siPRMT1, were treated 6 h with R5020 (10 nM). Total RNA was prepared and complementary DNAs (cDNAs) were analyzed by RT-qPCR with primers for *EGFR*, *STAT5A*, and *FKBP5*. Mean values were normalized against the expression of 28S ribosomal mRNA as reference. The p value was calculated using a paired t test: * indicates $p \leq 0.05$, ** $p \leq 0.01$, and *** $p \leq 0.001$. All the graphs show mean ± SEM for, at least, three independent experiments.

luciferase-based transcription assay established that PRMT1 enhanced reporter gene activity of PR and that its enzymatic function was required for this effect (Figure 4A). We next asked whether PRMT1 was recruited to some PR-binding sites, identified by genome-wide mapping of, in T47D cells stimulated with R5020 (Ballaré et al., 2013; Kougioumtzi et al., 2014). Chromatin immunoprecipitation experiments followed by qPCR analysis (ChIP-qPCR) were performed in T47D cells stimulated with R5020 (or vehicle ethanol) for 1 h. Figures 4B–4D illustrate the recruitment of PRMT1, as well as PR and the activation mark H3K4me3, to chromatin PR-binding sites of three endogenous well-characterized progesterone target genes, *EGFR*, *STAT5*, and *FKBP5* (Ballaré et al., 2013; Vicent et al., 2013). To analyze the expression of these genes, starved T47D cells were treated with R5020 and mRNAs were collected several times after the treatment. By quantitative real-time RT-PCR (RT-qPCR), we found a robust mRNA expression at 6 h (Figure S3A), and we chose this time for the remaining experiments. To determine whether PRMT1 was a coregulator of endogenous PR, we knocked down PRMT1 in T47D cells using a pool of three specific siRNAs and examined the expression of these PR target genes. RT-qPCR measurements revealed that, compared with the untreated cells, PRMT1 depletion differentially affected the expression of these PR-target genes: *EGFR* gene expression was decreased, *STAT5* mRNA level was increased, whereas *FKBP5* expression was not significantly changed (Figure 4E). As such, the impact of PRMT1 on the PR-dependent transcription appears to be gene specific. We confirmed the effect of PRMT1 depletion on the PR-dependent transcription in a second PR-positive breast cancer cell line, ZR-75 (Figures S3B and S3C).

PRMT1 Is Required for Progestin-Induced Expression of PR Target Genes Regulating Cell Growth and Migration and Predicts Poor Survival in Patients with Breast Cancer

To address the relevance and the functional significance of the above results, we performed RNA sequencing (RNA-seq) analyses using PRMT1-depleted T47D cells by siRNAs, stimulated 6 h with R5020 treatment (Figure 5A, left panel). The efficacy of hormonal treatment and PRMT1 knockdown were confirmed by IB and RT-qPCR (Figures S4A–S4C). RNA-seq results indicated that, among the 795 genes activated after hormonal exposure (Figure 5A, right panel, pink color), 235 genes were impacted by siPRMT1 (about 30% of the total R5020-regulated genes) (Figure 5A, red color). Among those, 64% of genes were downregulated when PRMT1 expression was decreased, indicating that their R5020-induced activation required PRMT1 (PRMT1-activated genes). Conversely, 36% are characterized as PRMT1-repressed genes (Figure 5B). RT-qPCR analysis of genes randomly selected from the list of PRMT1-dependent genes confirmed that PRMT1 is required for their R5020-induced transcription (Figure S4D). Among the 235 genes regulated by R5020 and PRMT1, we analyzed *EGFR*, *EGR1*, *SGK1*, and *CD44*, which are functionally connected and described for their roles in the regulation of mammary epithelium differentiation under normal physiology and in cell migration and invasion during breast cancer progression (Figure S4E) (Kovacevic et al., 2016; Menezes et al., 2017). RT-qPCR and IB analysis confirmed that depletion of PRMT1 significantly reduced the R5020-dependent expression of these key targets (Figures 4E and 5C). Of interest, PRMT1 knockdown also inhibited the phosphorylation of PDK1 and p38 MAPK, two enzymes involved in the activation of SGK1 (Liu et al., 2019), leading to the activation of downstream targets, such as *NDRG1* (Castel et al., 2016; Godbole et al., 2018; McCaig et al., 2011) (Figures 5D and S4F). To rule out the possibility of off-target effects and further confirm the specificity of the PRMT1 silencing, we expressed a tagged form of rat PRMT1 cDNA (flag-PRMT1, resistant to siRNAs silencing) in PRMT1-silenced cells. In this rescue experiment, we found that the expression of PRMT1 restored the expression of previously tested genes affected by PRMT1 knockdown, almost to the levels of control cells (Figures 5E, S4G, and S4H). Altogether, these data strongly indicate that PRMT1 silencing is specific and reversible.

Moreover, a pathway analysis of the 235 differentially regulated genes obtained by RNA-seq (list given in Table S1) revealed an enrichment of genes involved in cell movement, morphology, and proliferation (Figure 6A). Consistently, depletion of PRMT1 significantly reduced the proliferation and the cellular migration of R5020-stimulated T47D cells, compared with the vehicle (eth)-treated cells, both analyzed with Incucyte technology (Figures 6B, 6C, and S5A–S5C). To support these phenotypes, we then investigated the

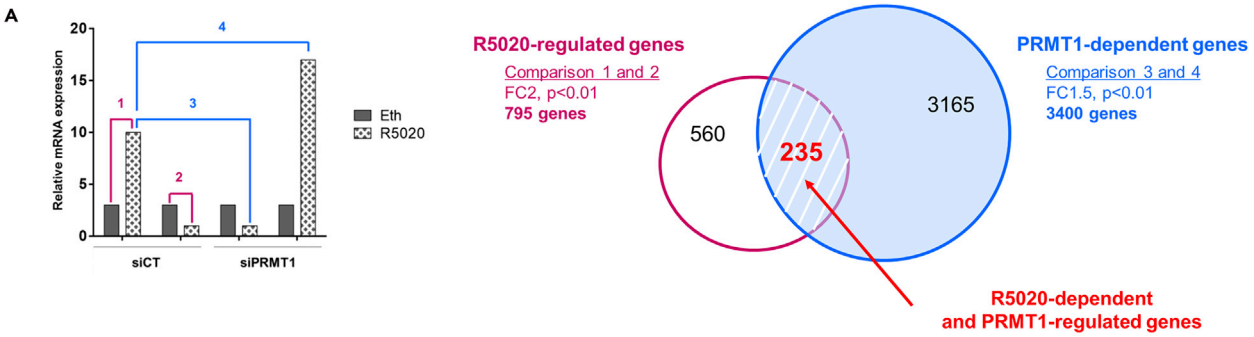
A
Relative mRNA expression
Eth
R5020
siCT
siPRMT1
R5020-regulated genes
Comparison 1 and 2
FC2, p<0.01
795 genes
PRMT1-dependent genes
Comparison 3 and 4
FC1.5, p<0.01
3400 genes
560
235
3165
R5020-dependent
and PRMT1-regulated genes

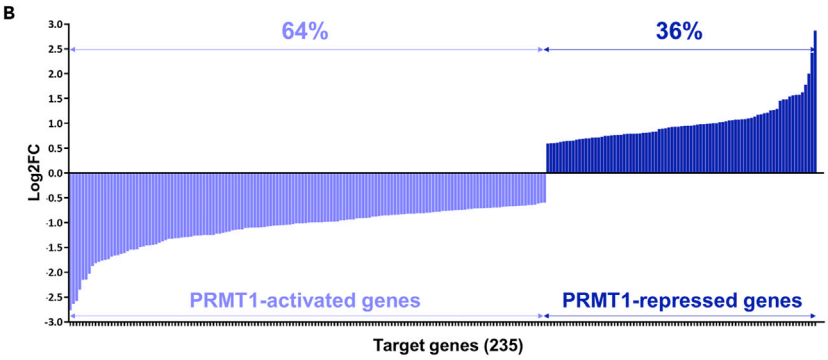
B
64%
36%
Log2FC
PRMT1-activated genes
PRMT1-repressed genes
Target genes (235)

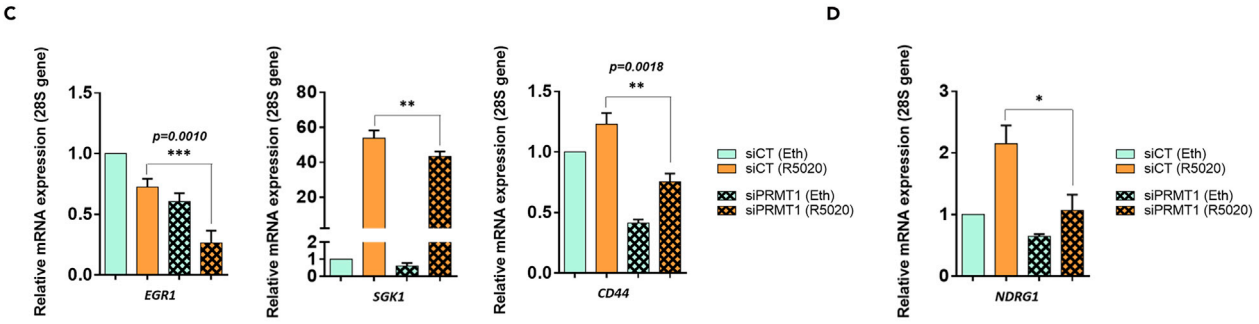
C
D
Relative mRNA expression (28S gene)
p=0.0010
***
EGR1
**
SGK1
p=0.0018
**
CD44
*
NDRG1
siCT (Eth)
siCT (R5020)
siPRMT1 (Eth)
siPRMT1 (R5020)

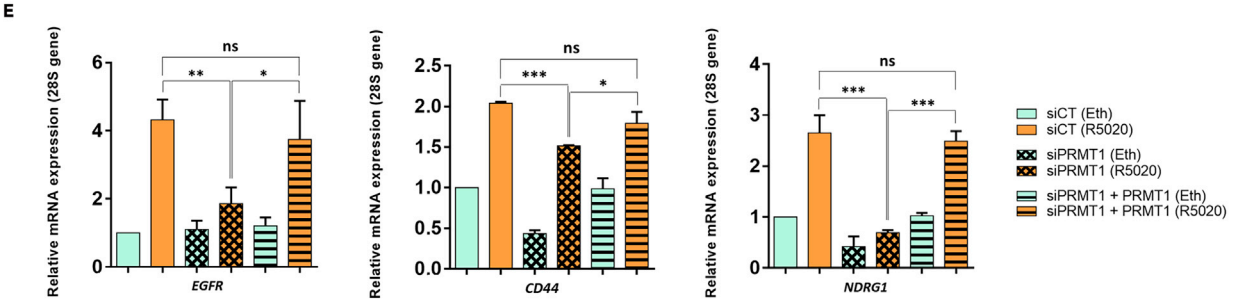
E
Relative mRNA expression (28S gene)
ns
**
*
EGFR
***
CD44
NDRG1
siCT (Eth)
siCT (R5020)
siPRMT1 (Eth)
siPRMT1 (R5020)
siPRMT1 + PRMT1 (Eth)
siPRMT1 + PRMT1 (R5020)

Figure 5. PRMT1 Is Required for Progesterone-Dependent Expression of a Subset of PR Target Genes

(A) Genome-wide RNA-seq analysis was performed using T47D cells to identify genes dependent on PRMT1 for R5020-regulated expression. Left panel: Hypothetical results of gene expression profiles for a given gene, illustrating how specific pairwise comparisons were performed between datasets for individual samples. Numbered bars represent hypothetical mRNA levels from RNA-seq data for cells expressing the indicated siRNAs (PRMT1 or CT) and treated for 6 h with ethanol (Eth) or R5020 (10 nM). Colored numbers represent pairwise comparisons performed to determine sets of genes for which mRNA levels were significantly different between the samples. For instance, comparison 1 = set of R5020-regulated genes (fold change $\geq$2, adjusted $p < 0.01$); comparison 4 = set of PRMT1-dependent genes (fold change >1.5, adjusted $p < 0.01$). Right panel: Pink and white Venn diagram represents the R5020-regulated genes in cells expressing siCT (comparisons 1 and 2); blue Venn diagram for PRMT1-dependent genes in R5020-treated cells (comparisons 3 and 4). Overlap area (in red) indicates the number of genes shared among sets. Controls for T47D cell treatments are provided in the Figures S4A–S4C.

(B) Representation of fold changes (log2FC) of all target gene expressions identified by RNA-seq analysis (235 genes). On the left (light blue), genes that are downregulated with siPRMT1 (64%), thus positively regulated by PRMT1. On the right (dark blue), genes that are negatively regulated by PRMT1 (36%).

(C and D) T47D cells were transfected with siRNAs against PRMT1 (or control) and treated for 6 h with ethanol (Eth) or R5020 (10 nM). Total RNA was prepared and cDNAs were analyzed by RT-qPCR with the indicated primers.

(E) cDNAs of T47D cells transfected with anti-PRMT1 siRNAs and co-transfected with a plasmid expressing a rat-PRMT1, then treated for 6 h with R5020 (10 nM) or vehicle ethanol (Eth), were analyzed by RT-qPCR.

All the cDNA mean values were normalized against the expression of 28S ribosomal mRNA as reference. Results shown are mean $\pm$ SEM for, at least, three independent experiments. The p value was calculated using a paired t test: * indicates $p \leq 0.05$, ** $p \leq 0.01$ and *** $p \leq 0.001$.

correlation between PR and PRMT1 expression and patient survival, in a cohort of 1,764 breast tumors expression, by Kaplan-Meyer survival analysis (Győrffy et al., 2010). After confirming that high-PR expression tumors depicted a better relapse-free survival (RFS) in this cohort, compared with low-PR expression ones (Figure 6Da), patients were separated into two groups according to PRMT1 expression (low and high PRMT1 following the median). Interestingly, patients with high expression of PR but low expression of PRMT1 reflected a significantly longer RFS ($p = 1 \times 10^{-11}$) (Figure 6Db). Similar observations were done with overall (OS) ($p = 0.00012$) and distal metastasis-free survival (DMFS) ($p = 1 \times 10^{-4}$) (Figures S5Db and S5Eb). Collectively, these results underscore that, in PR-positive tumors, low level of PRMT1, causing a decreased expression of some PR target genes including *EGFR* and *EGR1*, can inhibit cell proliferation and migration in hormonally responsive breast cancer, leading to a better survival outcome for patients (Figures 6D, S5D, and S5E).

Loss of PR Methylation at R637 Affects PR Degradation and T47D Cell Proliferation

To directly investigate the function of PRMT1-dependant PR methylation in cells, we used the CRISPR-Cas9 technology in T47D cells. We first knocked out endogenous PR, and the characterization of representative PR KO clones (T47D PR_{KO}) is illustrated in Figures S6A and S6B. Next, we stably re-expressed the wild-type (WT) and mutated (R637K) forms of PR-B in the T47D PR_{KO} cells and named these derived cell lines $T47D_{WT}$ and $T47D_{R637K}$, respectively. The cellular localization of WT- and R637K-PR proteins was analyzed by immunofluorescence using an anti-PR antibody (Figure 7A). We showed that, in both $T47D_{WT}$ and $T47D_{R637K}$ cell lines, the receptor was correctly localized in the nucleus (Figure 7A). Importantly, we also confirmed that PR was dimethylated after hormonal treatment in $T47D_{WT}$ cells, whereas in $T47D_{R637K}$ cells, the methylation signal was strongly reduced (Figure 7B). Together, these results confirm not only that these cell lines are functionally comparable with the native T47D cells but also that the R637 is the major methylated residue of PR.

Using these two cell lines, we analyzed the impact of the R637K mutation on progesterone signaling. As expected, treatment of $T47D_{WT}$ and $T47D_{R637K}$ cells with R5020 induced a rapid and transient activation of ERK kinases (Figure 7C). However, as observed after PRMT1 depletion, the mutation affected ERK activation, even if to a lesser extent (see Figure 3A). As with PRMT1 inhibition, loss of PR methylation at R637 resulted in a higher basal PR protein level, which appeared stable after R5020 stimulation (Figures 7A–7C). Cycloheximide treatment showed that more than 90% of PR-R637K was still present after 6 h of R5020 exposure, compared with less than 50% in $T47D_{WT}$ cells (Figure 7D). The difference in protein level is caused by the shorter half-life of the wild-type PR compared with the mutant, which corresponds to the increased steady-state level of PR-R637K. Thus, PRMT1-mediated methylation seems to participate in the regulation of PR turnover, required for active hormonal-dependent transcription (Métivier et al., 2003). In line with these results, absence of PR methylation at R637 markedly decreased oncogenic PR functions, leading to reduced cell growth and colony formation of $T47D_{R637K}$ cells, compared with $T47D_{WT}$ cells, when treated with R5020 (Figures 7E, 7F, and S6C). Importantly, expression of some PRMT1-dependent PR-downstream targets identified in Figure 5, as EGFR and EGR1, appeared lower in $T47D_{R637K}$ cells, after progesterone induction (Figures 7G and 7H).

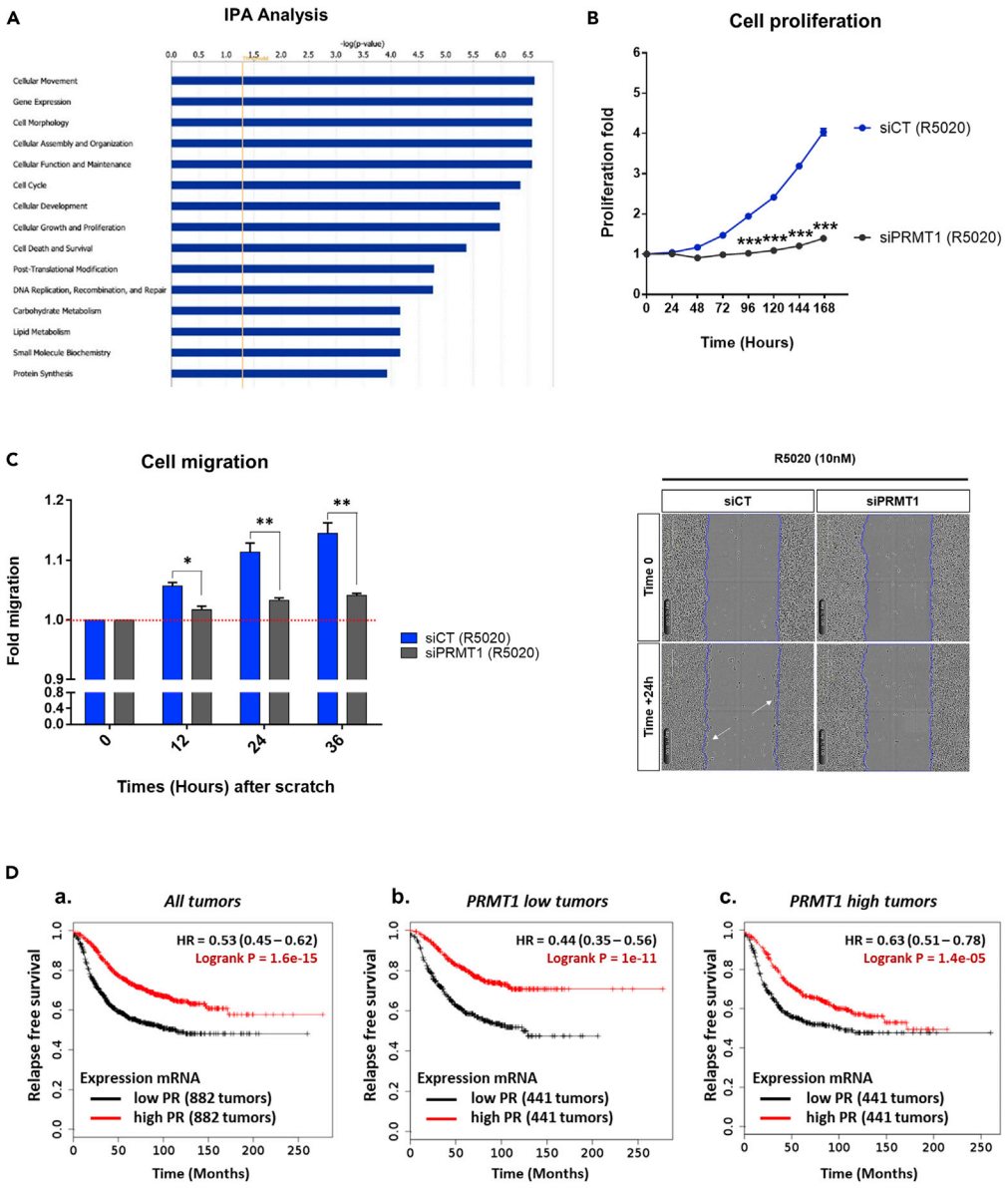

Figure 6. Low PRMT1 Reduces R5020-Induced Proliferation and Migration of T47D Breast Cancer Cells and Predicts Improved Survival of Patients with Breast Cancer

(A) Ingenuity Pathway Analysis (IPA) of cellular functions for the 235 R5020-regulated genes dependent on PRMT1. The orange vertical line represents the fold of statistical significance.

(B) Analysis of T47D cell proliferation by Incucyte technology. Cells expressing the indicated siRNAs (PRMT1 or CT) were stimulated with R5020 (10 nM) every 48 h for 7 days. Image acquisition was conducted every hour using the Incucyte software, which calculates the percentage of cell confluency according to time over 7 days. Results are represented as a graph showing the proliferation rate every 24 h.

(C) Migration of T47D cells expressing the indicated siRNAs (PRMT1 or CT) and treated with R5020 (10 nM) for 12, 24, and 36 h was analyzed in a wound scratch assay with the Incucyte Live-Cell Imaging System and dedicated software (Essen Bioscience), as reported in the Transparent Methods section. Left panel: The bar plots indicate the cellular migration rate, with a direct comparison between control and PRMT1-depleted cells. Right panel: Images of cells 24 h after the scratch wound. The blue line corresponds to the initial area of the wound. White arrows indicate cell migration areas. Both (B) and (C) graphs show the mean ± SD of one experiment representative of three. The p value was determined using the Student's t test: * indicates $p \leq 0.05$, ** $p \leq 0.01$, and *** $p \leq 0.001$.

(D) Kaplan-Meier estimates relapse-free survival in patients, in GEO, EGA, TCGA datasets, with low (black) or high (red) PR expression, as indicated using KM-plotter in a cohort of 1,764 breast tumors (a), or stratified in 2 groups following low-PRMT1 (b) or high-PRMT1 expression (c).

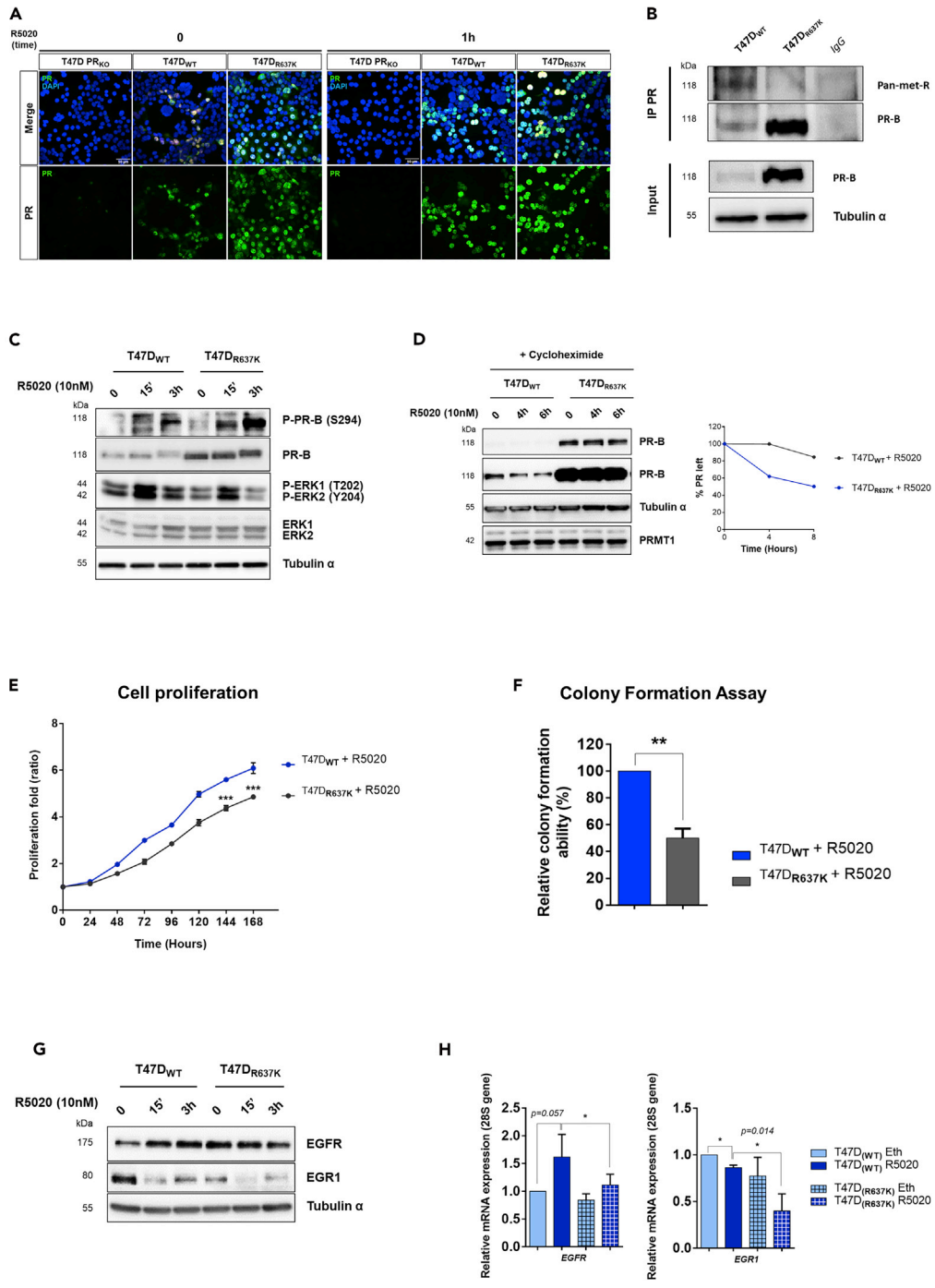

Figure 7. Inhibiting PR Methylation Affects Breast Cancer Cell Proliferation and PR Stability

(A) Immunofluorescence of T47D PR_{KO}, $T47D_{WT}$, and $T47D_{R637K}$ cells, before and after stimulation with 10 nM of R5020, stained with anti-PR antibody. The nuclei were counterstained with DAPI (blue) (Obj: X40).

(B) WCE of $T47D_{WT}$ or $T47D_{R637K}$, stimulated with R5020 (10 nM) for 1 h, were used for IP with anti-PR antibody or control IgG and immunoblotted with pan-meth-R and PR antibodies.

(C) WCE from $T47D_{WT}$ and $T47D_{R637K}$ cells stimulated with R5020 for the indicated times were immunoblotted.

(D) Half-life of the endogenous PR in $T47D_{WT}$ and $T47D_{R637K}$ cells. Left panel: WCE from $T47D_{WT}$ and $T47D_{R637K}$ cells treated with cycloheximide before the stimulation with R5020 were immunoblotted with the indicated antibodies. The amount of PR was quantified by densitometry; two different expositions are shown to well quantify the PR band intensity

Figure 7. *Continued*
for each time. Right panel: The half-life curves for each cell line is graphically represented. This experiment is representative of three independent experiments.
(E) Analysis of $T47D_{WT}$ and $T47D_{R637K}$ cell proliferation by Incucyte technology, performed as described in Figure 6B.
(F) $T47D_{WT}$ and $T47D_{R637K}$ cells were stimulated with 10 nM of R5020, and colony growth was measured at 10 days after staining with crystal violet. Both (E) and (F) graphs show the mean ± SD of one experiment representative of three. The p value was determined using the Student's t test: ** indicates $p \leq 0.01$ and ***$p \leq 0.001$.
(G and H) $T47D_{WT}$ and $T47D_{R637K}$ cells were stimulated with R5020 (10 nM). EGFR and EGR1 expression were analyzed (G) by IB and (H) by RT-qPCR (after 6 h of R5020 induction). The mean ± SEM of, at least, three independent experiments is shown. The p value was calculated using a paired t test: * indicates $p \leq 0.05$.

Interestingly, the loss of R637 methylation consequences observed under progesterone treatment are similar to those obtained with PRMT1-knockdown cells, suggesting that PRMT1 effects on the progesterone pathway occur, at least in part, through the methylation of PR.

DISCUSSION

Our study highlights the direct and functional cross talk between PRMT1, arginine methylation, and progesterone signaling, uncovering the molecular mechanisms by which PRMT1 functions as an important modulator of the progesterone response pathway. In the context of hormonal activation, we demonstrated that PRMT1 is recruited on PR-associated chromatin regions of some progestin-regulated genes. RNA-seq data support these results, showing that PRMT1 knockdown in breast cancer cells can affect the expression of thousand progesterone-targeted genes, positively or negatively. Moreover, PRMT1-regulated genes are involved in relevant cell functions including cell movement, morphology, and proliferation. We notably showed that PRMT1 positively regulates the expression of a subset of genes involved in the regulation of cell migration and invasion during breast cancer progression. Consistently, silencing of PRMT1 in T47D cells leads to a significant reduced ability to proliferate and migrate, supporting the involvement of PRMT1 in breast tumorigenesis. Therefore, it is possible that high-level expression of PRMT1 facilitates oncogenesis by providing tumor cells with a survival advantage, in part by enhancing the progestin-dependent receptor degradation and thereby maintaining cells in a proliferative mode. In line with this idea, the analysis of PRMT1 prognostic value in patients with breast cancer showed that high expression of PRMT1 associated with high expression of PR predicts poor relapse-free (RFS), overall (OS), and distal metastasis-free survival (DMFS). This suggests that PRMT1 expression influences the survival of patients with PR-positive breast cancer and that the prognostic value and pathophysiological role of PR depend on PRMT1 expression.

Many studies have already revealed the impact of PRMT1 in breast tumorigenesis (Liu et al., 2019; Morettin et al., 2015). Its expression is often upregulated in tumor samples compared with adjacent normal tissue. Moreover, these studies have highlighted different mechanisms by which PRMT1 regulates the proliferation of tumor cells (regulation of the epithelio-mesenchymal transition EMT, sensitization of cells to a therapy, etc.) (Yang and Bedford, 2013). Here, we report that the direct methylation of the progesterone receptor, a key driver of breast cells proliferation, affects breast cancer progression. Since PRMT1 enhances the transcriptional activity of PR (Figure 4A), we can consider that PRMT1-mediated transactivation is mainly due to direct methylation of PR, leading to increased transcription via the tight control of PR turnover. This is supported by the biological consequences of PR methylation at R637 under physiological conditions, using the $T47D_{WT}$ and $T47D_{R637K}$ cell lines, engineered to stably express the wild-type and mutant forms of PR-B in PR_{KO} T47D cells. We established that the effects of the methylation loss at R637 are consistent with the results obtained in PRMT1 knocked-down cells: $T47D_{R637K}$ cells display decreased oncogenic PR functions, such as a retarded cell growth and a reduced expression of some PRMT1-dependent PR downstream targets identified by RNA-seq (Figures 5 and 7). Moreover, the methylation of R637 directly affects PR stability (Figure 7), suggesting that PRMT1 effects on progesterone pathway occur, at least in part, through the methylation of PR on this conserved residue. Notably, the arginine R637 is located within the hinge region of the steroid receptor, which contains sites for posttranslational modifications, like phosphorylation and acetylation. Precisely, this conserved R637 flanks an acetylation consensus site, in which three lysine residues K638-640-641 are modified following progesterone stimulation (Daniel et al., 2010). It is interesting to note that non-acetylatable mutants ($PR_{K\text{-}A}$) exhibit defective transcriptional activation and are more stable than wild-type receptors, namely, a phenotype similar to the non-methylable mutant PR_{R637K} (Figure 7). Thus, it could exist as a functional communication

between these two modifications, as we currently observed with the histone tails on chromatin (Bannister and Kouzarides, 2011).

In response to ligand binding, MAPK activation modulates PR activity by phosphorylating the receptor on serine 294 (Lange et al., 2000; Shen et al., 2001). This modification is crucial for PR nuclear activity, priming the receptor for robust transcriptional activation, also influencing its promoter selectivity (Daniel et al., 2009). Our report demonstrates that progestin treatment induces the recruitment of PRMT1 on several PR-target genes, implying that PRMT1 acts as a coregulator of PR. Furthermore, we also describe that PRMT1 directly dimethylates PR under progestin treatment, primarily at the conserved R637 residue on an RGG methylation consensus motif, *in vitro* and *in vivo* (Figures 2D–2I). This methylation occurs in the nucleus and facilitates PR degradation, which in turn speeds up its transcriptional properties. Previous studies have demonstrated the critical role of PR degradation/re-synthesis in the active transcription of the receptor (Dennis et al., 2005). Indeed, the degradation constitutes a stimulatory switch that accelerates the recycling of receptors from pre-initiation complexes, required for active hormonal-dependent transcription (Métivier et al., 2003). Our results show that this mechanism involves the asymmetric dimethylation of PR by PRMT1, which reduces PR stability by affecting the proteasome machinery, thereby accelerating its transcriptional activity. It is tempting to speculate that the effects of PRMT1 on PR degradation/stability can be mediated by a cross talk with PR ubiquitination. Interestingly, recent data have shown that the RNA-binding protein RBM15 is methylated by PRMT1, which triggers its ubiquitination and degradation by the E3 ligase CNOT4 (Zhang et al., 2015). CNOT4 is a subunit of the CCR4-NOT complex (Albert et al., 2002), and we previously showed that PRMT1 physically interacts with the CCR4-NOT complex, regulating its methyltransferase activity (Chapat et al., 2017; Robin-Lespinasse et al., 2007). In future studies, it will be interesting to investigate whether PRMT1-dependent methylation of PR induces its degradation through the recruitment of the E3 ligase CNOT4.

In conclusion, our findings reveal important insights linking PRMT1-dependent arginine methylation to the maintenance of the balance between transcriptional activity and degradation of PR. This result implies that altered methylation of the receptor can induce aberrant cellular response to hormonal stimuli contributing to pathogenesis. However, most of the mechanisms described above are based on *in vitro* experiments, obtained using a breast cancer cell line with a phenotype particularly useful to dissect the regulatory steps of progesterone signaling, independently of the estrogen receptor (ERα). Future studies will be needed in preclinical models, notably mouse and patient-derived xenografts or directly in patient samples, to determine the clinical relevance of our *in vitro* mechanistic findings. In addition, improved knowledge of these mechanisms could have a significant impact on long-term outcome for patients with breast cancer, considering the differential effects of progesterone in breast cancers. In fact, recent studies (Finlay-Schultz et al., 2017; Mohammed et al., 2015) indicate that functional relationships between ERα and PR signaling occur in ER^+/PR^+ breast cancers. Indeed, PR can inhibit the growth-promoting functions of estrogen by directly reprogramming chromatin binding of ERα or indirectly, by reducing the bio-availability of molecules needed for tumor growth. These new findings may provide additional strategies to treat ERα-positive breast cancer, by modulating the interactions between ERα and PR. Given that both receptors are regulated by PRMT1 *via* their direct methylation, and that PRMT1 clearly influences the clinical outcome of breast cancer patients according to PR expression, we speculate that PRMT1 can be involved in the ERα/PR cross talk, whose mechanistic details are not yet well understood. Therefore, targeting PRMT1-mediated methylation may be a promising strategy for breast cancer treatments; the recent development of pre-clinical small molecules targeting PRMT1 (Fedoriw et al., 2019) may offer a path toward that goal.

Limitations of the Study

Our study depicts a new post-translational modification in the DNA-binding domain of the progesterone receptor, the arginine methylation, deposited by the enzyme PRMT1. Although our data highlight PRMT1 as a transcriptional coregulator of a subset of PR-target genes, involved in breast cancer cell proliferation and migration, we were unable to directly link the arginine methylation to this transcriptional effect. In fact, our home-made antibody specifically directed against the methylated form of PR did not give specific signal in chromatin immunoprecipitation (ChIP) experiment. Thus, we actually do not know if the methylated form of the receptor is bound to DNA and if the methylation affects the association between PR and its coregulators. Most of the molecular mechanisms described in this article come from *in vitro* studies using the PR-positive cell line T47D, which permits to dissect the PR progesterone

signaling in the presence of progestin only and thus independently of ERα. On the contrary, recent studies have shown that estrogen and progestin have different biological consequences when analyzed individually or when both hormones are present, as these hormonal receptors are functionally interconnected. Therefore, these mechanistic studies need to be validated using more physiological preclinical models, such as mouse and patient-derived xenografts, or directly in patient samples, to assess their clinical relevance.

Resource Availability

Lead Contact

Further information and requests for resources and reagents should be directed to and will be fulfilled by the Lead Contact, Laura Corbo (laura.corbo@lyon.unicancer.fr).

Materials Availability

All unique reagents generated in this study (CRISPR cell lines, primers, plasmids) are available from the Lead Contact without restriction. There are restrictions for the availability of the methylated-R637-PR antibody, owing to our inability to produce it and our need to maintain the stock.

Data and Code Availability

RNA-seq data have been submitted to Gene Expression Omnibus (GEO) and are available with the GSE134194 submission number.

Original membranes for all the immunoblots presented in the paper have been deposited to Mendeley Data: [https://doi.org/10.17632/rgctdkjyzx.2].

METHODS

All methods can be found in the accompanying Transparent Methods supplemental file.

SUPPLEMENTAL INFORMATION

Supplemental Information can be found online at https://doi.org/10.1016/j.isci.2020.101236.

ACKNOWLEDGMENTS

We thank Helene Joly for starting the project and Julien Jacquemetton, Farida Nasri, Maéva Ruel, and Aurore Souef for helpful technical assistance. We are grateful to Dr. Loredana D'Amato, Dr. Samuele Gherardi, and Dr. Romain Teinturier for their valuable advice and discussions. We also thank Prof. Pierre Chambon for kindly providing the pSG5PR-B and MMTV-Luc plasmids, Dr. Catherine Teyssier for the PRMT1 constructs, and Dr. Stéphane Ansieau for the plasmid pPRUpu. We are also grateful to Benjamin Gillet and Sandrine Hughes for performing the RNA sequencing at the IGFL platform in Lyon. A special thanks to Brigitte Manship and Clément Chapat for reading the manuscript. This study was partially supported by the "Ligue Nationale Contre le Cancer," the "Association pour la Recherche sur le Cancer," and the association "Odyssea Chambery." L.M. is supported by a fellowship from the French Ministry of Research and by the "Fondation ARC pour la Recherche sur le Cancer" and C.P. by the "Fondation de France."

AUTHOR CONTRIBUTIONS

L.C., M.L.R., and L.M. conceived the study, designed the experiments, and analyzed data. L.M. carried out most of the experiments, C.L. assisted with the experiments, I.M. performed the CRISPR experiments, C.P. and F.F. helped L.M. with bioinformatics analysis of RNA-seq data. M.L.R. and I.M. contributed to result discussions and provided material. L.C. coordinated the project. The manuscript was written by L.C., with a strong contribution from L.M.

DECLARATION OF INTERESTS

The authors have declared that no competing interest exist.

Received: March 17, 2020
Revised: May 13, 2020
Accepted: June 2, 2020
Published: June 26, 2020

REFERENCES

Abdel-Hafiz, H.A., and Horwitz, K.B. (2014). Post-translational modifications of the progesterone receptors. J. Steroid Biochem. Mol. Biol. *140*, 80–89.

Albert, T.K., Hanzawa, H., Legtenberg, Y.I.A., de Ruwe, M.J., van den Heuvel, F.A.J., Collart, M.A., Boelens, R., and Timmers, H.T.M. (2002). Identification of a ubiquitin-protein ligase subunit within the CCR4-NOT transcription repressor complex. EMBO J. *21*, 355–364.

Ballaré, C., Castellano, G., Gaveglia, L., Althammer, S., González-Vallinas, J., Eyras, E., Le Dily, F., Zaurin, R., Soronellas, D., Vicent, G.P., et al. (2013). Nucleosome-driven transcription factor binding and gene regulation. Mol. Cell *49*, 67–79.

Bannister, A.J., and Kouzarides, T. (2011). Regulation of chromatin by histone modifications. Cell Res. *21*, 381–395.

Beato, M., and Vicent, G.P. (2012). Impact of chromatin structure and dynamics on PR signaling. The initial steps in hormonal gene regulation. Mol. Cell. Endocrinol. *357*, 37–42.

Bedford, M.T., and Clarke, S.G. (2009). Protein arginine methylation in mammals: who, what, and why. Mol. Cell *33*, 1–13.

Blanc, R.S., and Richard, S. (2017). Arginine methylation: the coming of age. Mol. Cell *65*, 8–24.

Boonyaratanakornkit, V., Scott, M.P., Ribon, V., Sherman, L., Anderson, S.M., Maller, J.L., Miller, W.T., and Edwards, D.P. (2001). Progesterone receptor contains a proline-rich motif that directly interacts with SH3 domains and activates c-Src family tyrosine kinases. Mol. Cell *8*, 269–280.

Brisken, C., and O'Malley, B. (2010). Hormone action in the mammary gland. Cold Spring Harb. Perspect. Biol. *2*, a003178.

Castel, P., Ellis, H., Bago, R., Toska, E., Razavi, P., Carmona, F.J., Kannan, S., Verma, C.S., Dickler, M., Chandarlapaty, S., et al. (2016). PDK1-SGK1 signaling sustains AKT-independent mTORC1 activation and confers resistance to PI3Kα inhibition. Cancer Cell *30*, 229–242.

Chapat, C., Chettab, K., Simonet, P., Wang, P., De La Grange, P., Le Romancer, M., and Corbo, L. (2017). Alternative splicing of CNOT7 diversifies CCR4-NOT functions. Nucleic Acids Res. *45*, 8508–8523.

Daniel, A.R., Knutson, T.P., and Lange, C.A. (2009). Signaling inputs to progesterone receptor gene regulation and promoter selectivity. Mol. Cell. Endocrinol. *308*, 47–52.

Daniel, A.R., Gaviglio, A.L., Czaplicki, L.M., Hillard, C.J., Housa, D., and Lange, C.A. (2010). The progesterone receptor hinge region regulates the kinetics of transcriptional responses through acetylation, phosphorylation, and nuclear retention. Mol. Endocrinol. *24*, 2126–2138.

Dennis, A.P., Lonard, D.M., Nawaz, Z., and O'Malley, B.W. (2005). Inhibition of the 26S proteasome blocks progesterone receptor-dependent transcription through failed recruitment of RNA polymerase II. J. Steroid Biochem. Mol. Biol. *94*, 337–346.

Eram, M.S., Shen, Y., Szewczyk, M., Wu, H., Senisterra, G., Li, F., Butler, K.V., Kaniskan, H.Ü., Speed, B.A., Dela Seña, C., et al. (2016). A potent, selective, and cell-active inhibitor of human type I protein arginine methyltransferases. ACS Chem. Biol. *11*, 772–781.

Faivre, E.J., and Lange, C.A. (2007). Progesterone receptors upregulate Wnt-1 to induce epidermal growth factor receptor transactivation and c-Src-dependent sustained activation of Erk1/2 mitogen-activated protein kinase in breast cancer cells. Mol. Cell. Biol. *27*, 466–480.

Faivre, E.J., Daniel, A.R., Hillard, C.J., and Lange, C.A. (2008). Progesterone receptor rapid signaling mediates serine 345 phosphorylation and tethering to specificity protein 1 transcription factors. Mol. Endocrinol. *22*, 823–837.

Fedoriw, A., Rajapurkar, S.R., O'Brien, S., Gerhart, S.V., Mitchell, L.H., Adams, N.D., Rioux, N., Lingaraj, T., Ribich, S.A., Pappalardi, M.B., et al. (2019). Anti-tumor activity of the type I PRMT inhibitor, GSK3368715, synergizes with PRMT5 inhibition through MTAP loss. Cancer Cell *36*, 100–114.e25.

Finlay-Schultz, J., Gillen, A.E., Brechbuhl, H.M., Ivie, J.J., Matthews, S.B., Jacobsen, B.M., Bentley, D.L., Kabos, P., and Sartorius, C.A. (2017). Breast cancer suppression by progesterone receptors is mediated by their modulation of estrogen receptors and RNA polymerase III. Cancer Res. *77*, 4934–4946.

Godbole, M., Togar, T., Patel, K., Dharavath, B., Yadav, N., Janjuha, S., Gardi, N., Tiwary, K., Terwadkar, P., Desai, S., et al. (2018). Up-regulation of the kinase gene SGK1 by progesterone activates the AP-1-NDRG1 axis in both PR-positive and -negative breast cancer cells. J. Biol. Chem. *293*, 19263–19276.

Grimm, S.L., Hartig, S.M., and Edwards, D.P. (2016). Progesterone receptor signaling mechanisms. J. Mol. Biol. *428*, 3831–3849.

Győrffy, B., Lanczky, A., Eklund, A.C., Denkert, C., Budczies, J., Li, Q., and Szallasi, Z. (2010). An online survival analysis tool to rapidly assess the effect of 22,277 genes on breast cancer prognosis using microarray data of 1,809 patients. Breast Cancer Res. Treat. *123*, 725–731.

Hagan, C.R., Daniel, A.R., Dressing, G.E., and Lange, C.A. (2012). Role of phosphorylation in progesterone receptor signaling and specificity. Mol. Cell. Endocrinol. *357*, 43–49.

Helzer, K.T., Hooper, C., Miyamoto, S., and Alarid, E.T. (2015). Ubiquitylation of nuclear receptors: new linkages and therapeutic implications. J. Mol. Endocrinol. *54*, R151–R167.

Hill, K.K., Roemer, S.C., Jones, D.N.M., Churchill, M.E.A., and Edwards, D.P. (2009). A progesterone receptor co-activator (JDP2) mediates activity through interaction with residues in the carboxyl-terminal extension of the DNA binding domain. J. Biol. Chem. *284*, 24415–24424.

Jacobsen, B.M., and Horwitz, K.B. (2012). Progesterone receptors, their isoforms and progesterone regulated transcription. Mol. Cell. Endocrinol. *357*, 18–29.

Kastner, P., Krust, A., Turcotte, B., Stropp, U., Tora, L., Gronemeyer, H., and Chambon, P. (1990). Two distinct estrogen-regulated promoters generate transcripts encoding the two functionally different human progesterone receptor forms A and B. EMBO J. *9*, 1603–1614.

Kougioumtzi, A., Tsaparas, P., and Magklara, A. (2014). Deep sequencing reveals new aspects of progesterone receptor signaling in breast cancer cells. PLoS One *9*, e98404.

Knutson, T.P., and Lange, C.A. (2014). Tracking progesterone receptor-mediated actions in breast cancer. Pharmacol. Ther. *142*, 114–125.

Koh, S.S., Chen, D., Lee, Y.H., and Stallcup, M.R. (2001). Synergistic enhancement of nuclear receptor function by p160 coactivators and two coactivators with protein methyltransferase activities. J. Biol. Chem. *276*, 1089–1098.

Kovacevic, Z., Menezes, S.V., Sahni, S., Kalinowski, D.S., Bae, D.-H., Lane, D.J.R., and Richardson, D.R. (2016). The metastasis suppressor, N-MYC downstream-regulated gene-1 (NDRG1), down-regulates the ErbB family of receptors to inhibit downstream oncogenic signaling pathways. J. Biol. Chem. *291*, 1029–1052.

Lange, C.A., Shen, T., and Horwitz, K.B. (2000). Phosphorylation of human progesterone receptors at serine-294 by mitogen-activated protein kinase signals their degradation by the 26S proteasome. Proc. Natl. Acad. Sci. U S A *97*, 1032–1037.

Le Romancer, M., Treilleux, I., Leconte, N., Robin-Lespinasse, Y., Sentis, S., Bouchekioua-Bouzaghou, K., Goddard, S., Gobert-Gosse, S., and Corbo, L. (2008). Regulation of estrogen rapid signaling through arginine methylation by PRMT1. Mol. Cell *31*, 212–221.

Liu, L.-M., Sun, W.-Z., Fan, X.-Z., Xu, Y.-L., Cheng, M.-B., and Zhang, Y. (2019). Methylation of C/EBPα by PRMT1 inhibits its tumor-suppressive

function in breast cancer. Cancer Res. *79*, 2865–2877.

Mangelsdorf, D.J., Thummel, C., Beato, M., Herrlich, P., Schütz, G., Umesono, K., Blumberg, B., Kastner, P., Mark, M., Chambon, P., et al. (1995). The nuclear receptor superfamily: the second decade. Cell *83*, 835–839.

Mohammed, H., Russell, I.A., Stark, R., Rueda, O.M., Hickey, T.E., Tarulli, G.A., Serandour, A.A., Serandour, A.A.A., Birrell, S.N., Bruna, A., et al. (2015). Progesterone receptor modulates ERα action in breast cancer. Nature *523*, 313–317.

McCaig, C., Potter, L., Abramczyk, O., and Murray, J.T. (2011). Phosphorylation of NDRG1 is temporally and spatially controlled during the cell cycle. Biochem. Biophys. Res. Commun. *411*, 227–234.

Menezes, S.V., Sahni, S., Kovacevic, Z., and Richardson, D.R. (2017). Interplay of the iron-regulated metastasis suppressor NDRG1 with epidermal growth factor receptor (EGFR) and oncogenic signaling. J. Biol. Chem. *292*, 12772–12782.

Métivier, R., Penot, G., Hübner, M.R., Reid, G., Brand, H., Kos, M., and Gannon, F. (2003). Estrogen receptor-alpha directs ordered, cyclical, and combinatorial recruitment of cofactors on a natural target promoter. Cell *115*, 751–763.

Migliaccio, A., Piccolo, D., Castoria, G., Di Domenico, M., Bilancio, A., Lombardi, M., Gong, W., Beato, M., and Auricchio, F. (1998). Activation of the Src/p21ras/Erk pathway by progesterone receptor via cross-talk with estrogen receptor. EMBO J. *17*, 2008–2018.

Morettin, A., Baldwin, R.M., and Côté, J. (2015). Arginine methyltransferases as novel therapeutic targets for breast cancer. Mutagenesis *30*, 177–189.

Mulac-Jericevic, B., Lydon, J.P., DeMayo, F.J., and Conneely, O.M. (2003). Defective mammary gland morphogenesis in mice lacking the progesterone receptor B isoform. Proc. Natl. Acad. Sci. U S A *100*, 9744–9749.

Poulard, C., Treilleux, I., Lavergne, E., Bouchekioua-Bouzaghou, K., Goddard-Léon, S., Chabaud, S., Trédan, O., Corbo, L., and Le Romancer, M. (2012). Activation of rapid oestrogen signalling in aggressive human breast cancers. EMBO Mol. Med. *4*, 1200–1213.

Poulard, C., Rambaud, J., Le Romancer, M., and Corbo, L. (2014). Proximity ligation assay to detect and localize the interactions of ERα with PI3-K and Src in breast cancer cells and tumor samples. Methods Mol. Biol. *1204*, 135–143.

Poulard, C., Corbo, L., and Le Romancer, M. (2016). Protein arginine methylation/demethylation and cancer. Oncotarget *7*, 67532–67550.

Poulard, C., Jacquemetton, J., Pham, T.H., and Le Romancer, M. (2020). Using proximity ligation assay to detect protein arginine methylation. Methods *175*, 66–71.

Read, L.D., Snider, C.E., Miller, J.S., Greene, G.L., and Katzenellenbogen, B.S. (1988). Ligand-modulated regulation of progesterone receptor messenger ribonucleic acid and protein in human breast cancer cell lines. Mol. Endocrinol. *2*, 263–271.

Robin-Lespinasse, Y., Sentis, S., Kolytcheff, C., Rostan, M.-C., Corbo, L., and Le Romancer, M. (2007). hCAF1, a new regulator of PRMT1-dependent arginine methylation. J. Cell. Sci. *120*, 638–647.

Shen, T., Horwitz, K.B., and Lange, C.A. (2001). Transcriptional hyperactivity of human progesterone receptors is coupled to their ligand-dependent down-regulation by mitogen-activated protein kinase-dependent phosphorylation of serine 294. Mol. Cell. Biol. *21*, 6122–6131.

Smith, S.E., Mellor, P., Ward, A.K., Kendall, S., McDonald, M., Vizeacoumar, F.S., Vizeacoumar, F.J., Napper, S., and Anderson, D.H. (2017). Molecular characterization of breast cancer cell lines through multiple omic approaches. Breast Cancer Res. *19*, 65.

Söderberg, O., Gullberg, M., Jarvius, M., Ridderstråle, K., Leuchowius, K.-J., Jarvius, J., Wester, K., Hydbring, P., Bahram, F., Larsson, L.-G., et al. (2006). Direct observation of individual endogenous protein complexes in situ by proximity ligation. Nat. Methods *3*, 995–1000.

Stallcup, M.R., Chen, D., Koh, S.S., Ma, H., Lee, Y.H., Li, H., Schurter, B.T., and Aswad, D.W. (2000). Co-operation between protein-acetylating and protein-methylating co-activators in transcriptional activation. Biochem. Soc. Trans. *28*, 415–418.

Vicent, G.P., Nacht, A.S., Zaurin, R., Font-Mateu, J., Soronellas, D., Le Dily, F., Reyes, D., and Beato, M. (2013). Unliganded progesterone receptor-mediated targeting of an RNA-containing repressive complex silences a subset of hormone-inducible genes. Genes Dev. *27*, 1179–1197.

Vignon, F., Bardon, S., Chalbos, D., and Rochefort, H. (1983). Antiestrogenic effect of R5020, a synthetic progestin in human breast cancer cells in culture. J. Clin. Endocrinol. Metab. *56*, 1124–1130.

Wang, H., Huang, Z.Q., Xia, L., Feng, Q., Erdjument-Bromage, H., Strahl, B.D., Briggs, S.D., Allis, C.D., Wong, J., Tempst, P., et al. (2001). Methylation of histone H4 at arginine 3 facilitating transcriptional activation by nuclear hormone receptor. Science *293*, 853–857.

Yang, Y., and Bedford, M.T. (2013). Protein arginine methyltransferases and cancer. Nat. Rev. Cancer *13*, 37–50.

Zhang, L., Tran, N.-T., Su, H., Wang, R., Lu, Y., Tang, H., Aoyagi, S., Guo, A., Khodadadi-Jamayran, A., Zhou, D., et al. (2015). Cross-talk between PRMT1-mediated methylation and ubiquitylation on RBM15 controls RNA splicing. Elife *4*, e07938.

iScience, Volume *23*

Supplemental Information

PRMT1 Is Critical for the Transcriptional Activity and the Stability of the Progesterone Receptor

Lucie Malbeteau, Coralie Poulard, Cécile Languilaire, Ivan Mikaelian, Frédéric Flamant, Muriel Le Romancer, and Laura Corbo

A.

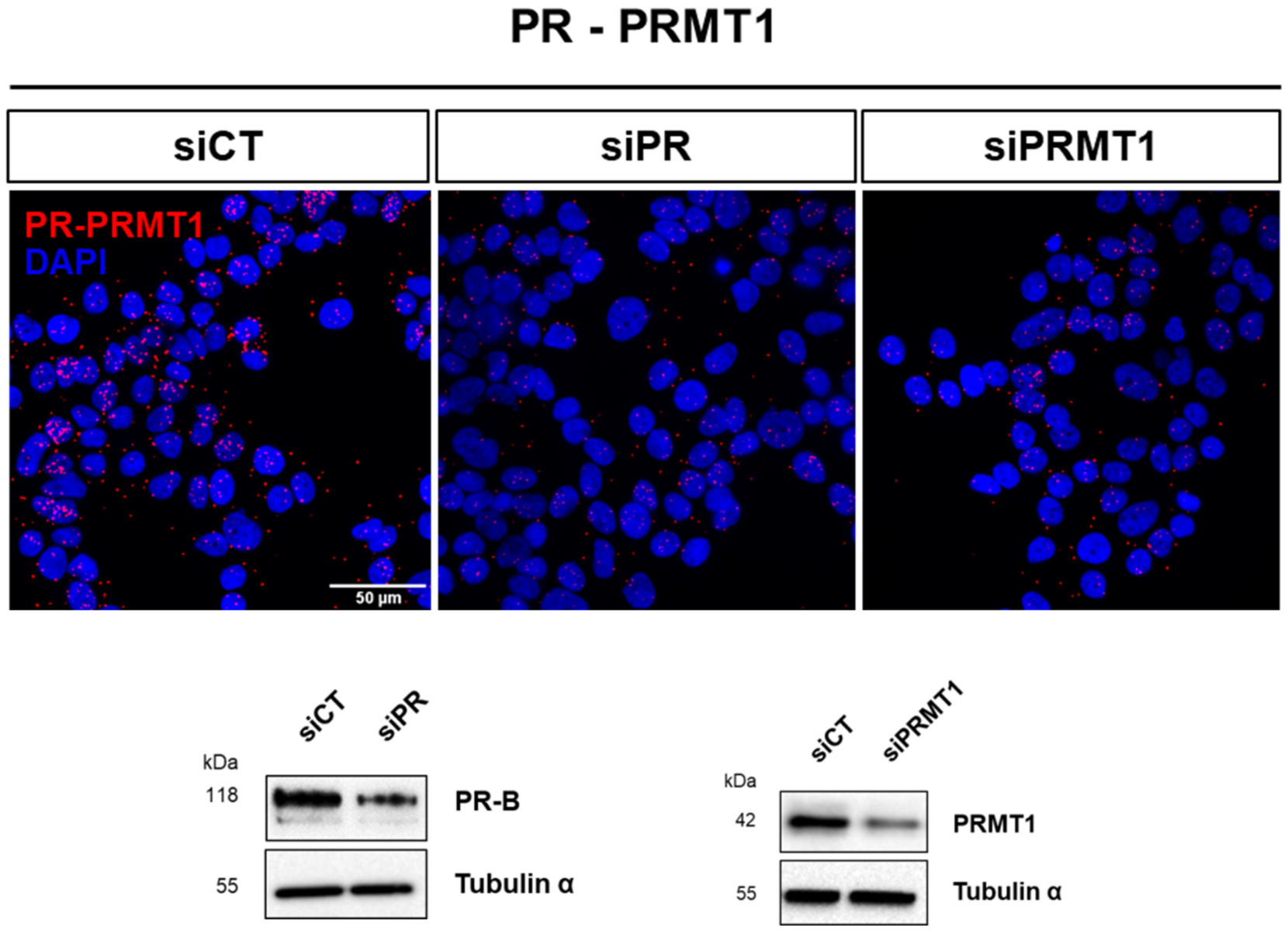
PR - PRMT1
siCT
siPR
siPRMT1
PR-PRMT1
DAPI
50 µm
siCT
siPR
kDa
118
PR-B
55
Tubulin α
siCT
siPRMT1
kDa
42
PRMT1
55
Tubulin α
Dots/cell
15
10
5
0
**
**
siCT
siPR
siPRMT1
T47D cells (Eth)

B.

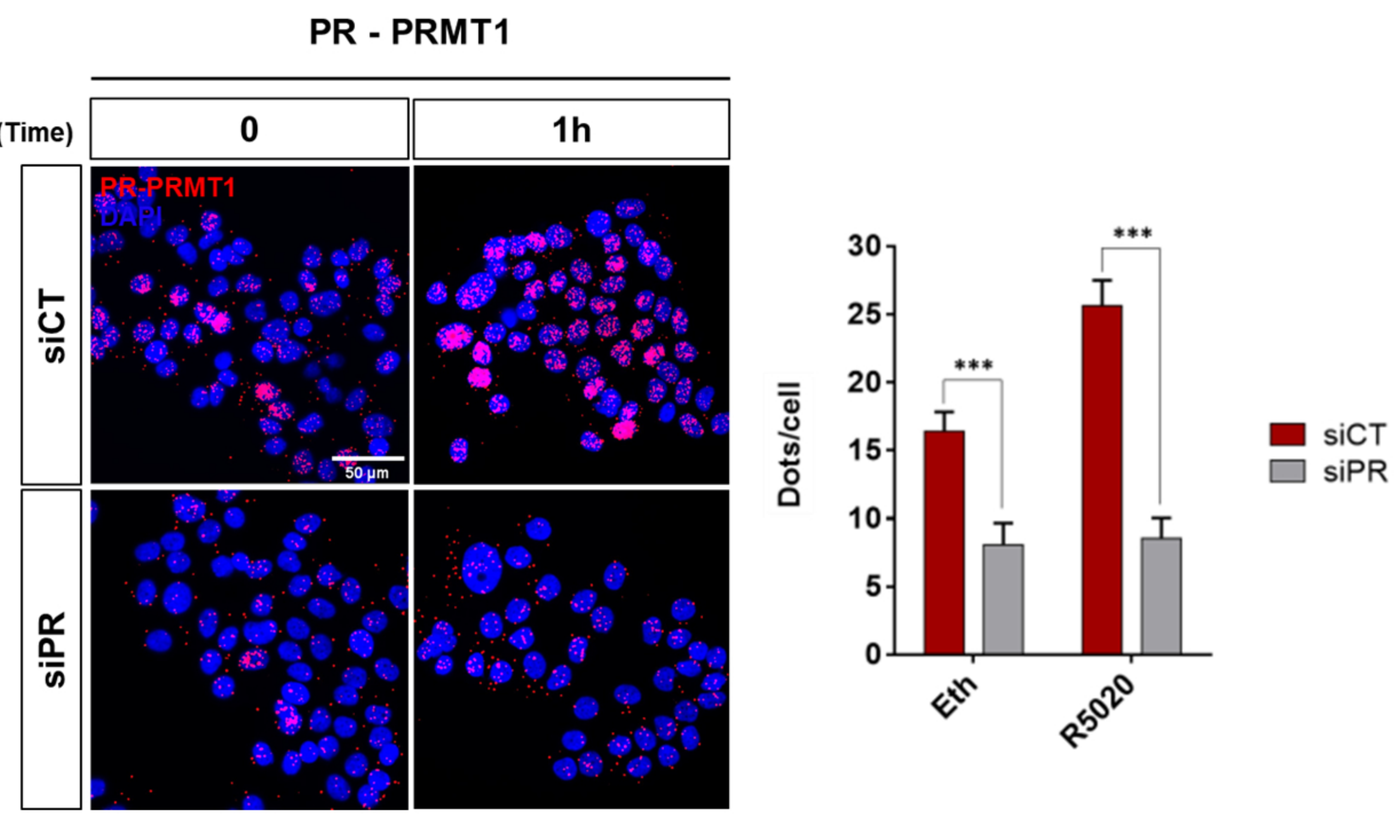
PR - PRMT1
R5020 (Time)
0
1h
siCT
siPR
PR-PRMT1
DAPI
50 µm
Dots/cell
30
25
20
15
10
5
0
***
***
Eth
R5020
siCT
siPR

C.

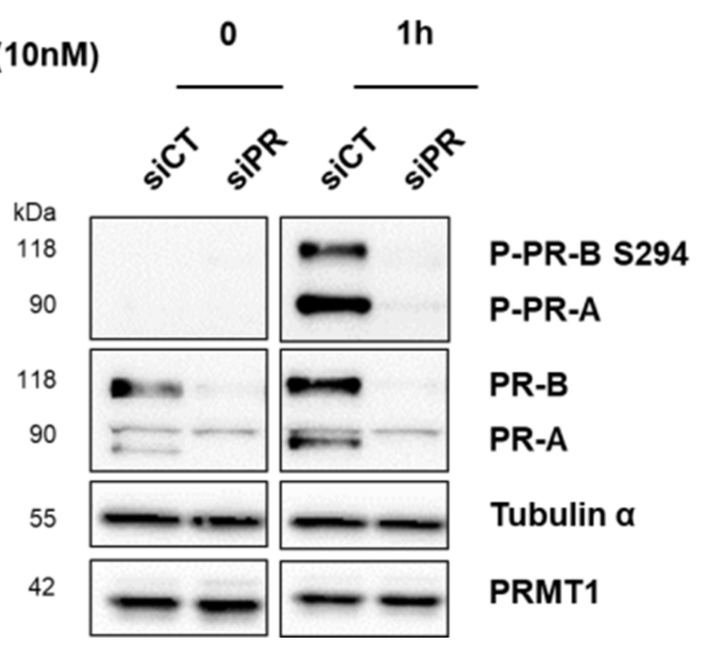
R5020 (10nM)
0
1h
siCT
siPR
siCT
siPR
kDa
118
90
P-PR-B S294
P-PR-A
118
90
PR-B
PR-A
55
Tubulin α
42
PRMT1

Figure S1, related to Fig. 1 | PRMT1 and PR interact in the nucleus of T47D breast cancer cells. Validation of the specificity of PRMT1-PR association detected by Ligation Assay (PLA). T47D were grown on coverslips in 12-well plates and transfected with siRNAs control (siCT) or against PR (siPR) or PRMT1 (siPRMT1). PLA was used to detect the cellular interaction of endogenous PRMT1 and PR **A.** in unstimulated cells or **B.** after R5020 treatment (1h). The interactions are represented by red dots. The nuclei were counterstained with DAPI (blue) (Obj: X60). Quantification of the number of signals per cell was performed by computer-assisted analysis, as reported in the Transparent Methods section, and is shown in the right panels. The mean ± SD of one experiment representative of three experiments is shown. The *p*-value was determined using the Student's t-test. ** indicates a $p \leq 0.01$ and *** indicates a $p \leq 0.001$. **C.** The efficacy of PRMT1- and PR-siRNAs treatments were analyzed by immunoblot.

A.

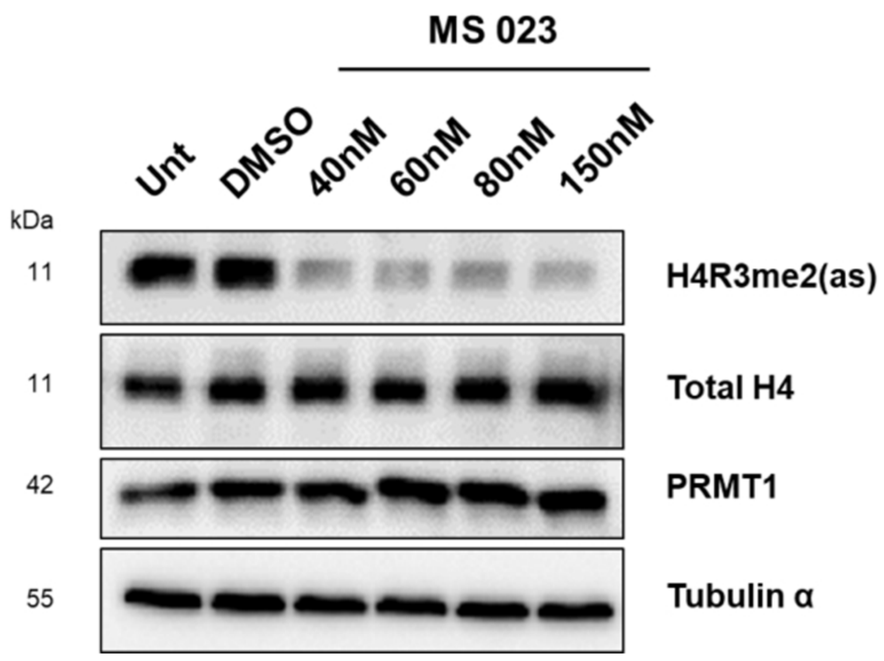
MS 023
Unt
DMSO
40nM
60nM
80nM
150nM
kDa
11
H4R3me2(as)
11
Total H4
42
PRMT1
55
Tubulin α

B.

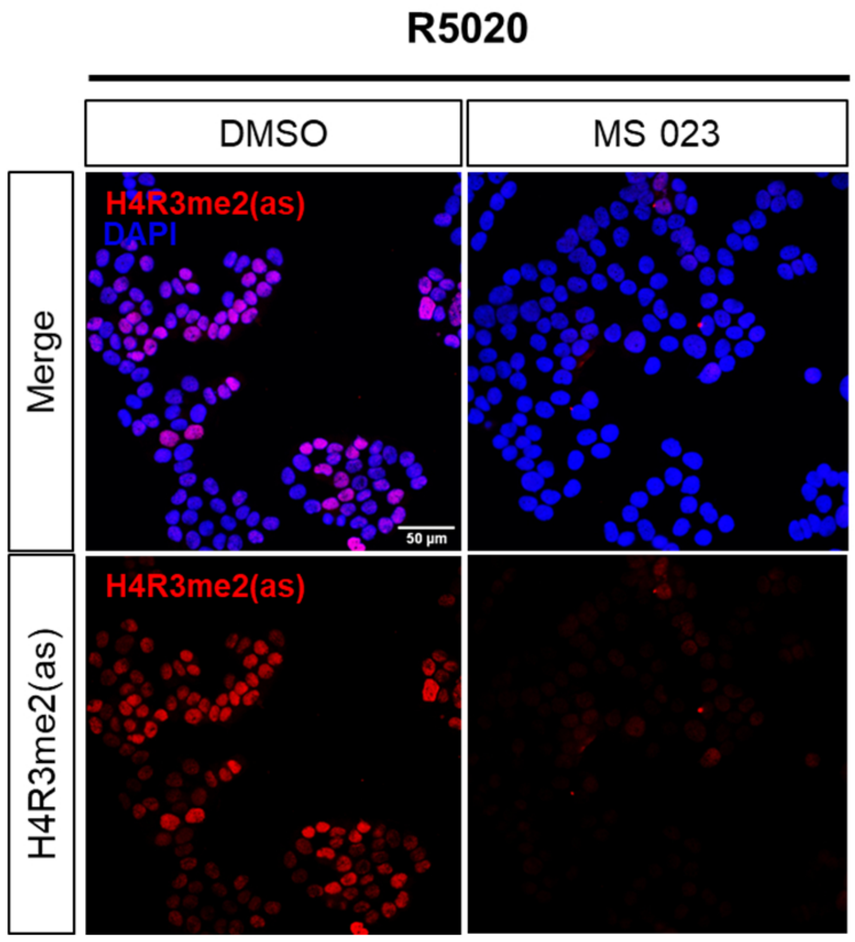
R5020
DMSO
MS 023
Merge
H4R3me2(as)
DAPI
50 μm
H4R3me2(as)
H4R3me2(as)

C.

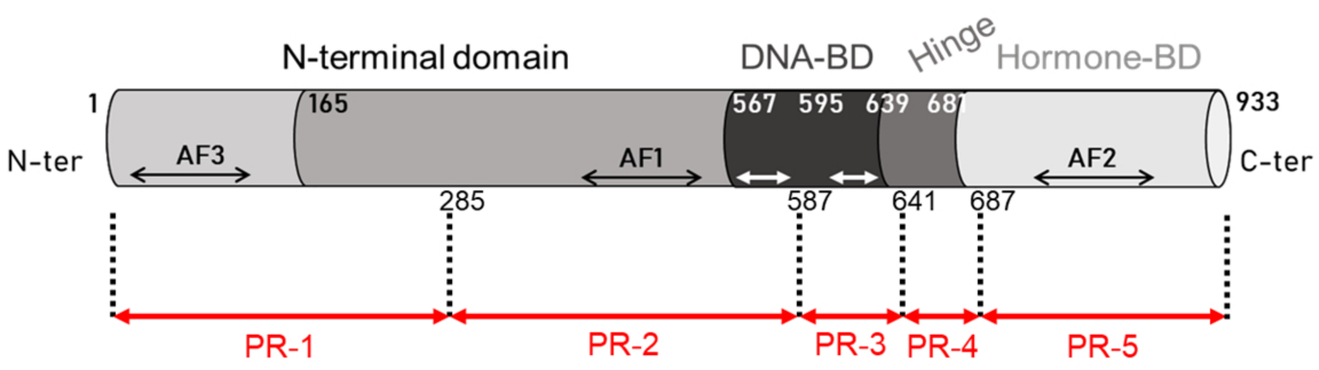
N-terminal domain
DNA-BD
Hinge
Hormone-BD
1
165
567
595
639
933
N-ter
AF3
AF1
AF2
C-ter
285
587
641
687
PR-1
PR-2
PR-3
PR-4
PR-5

D.

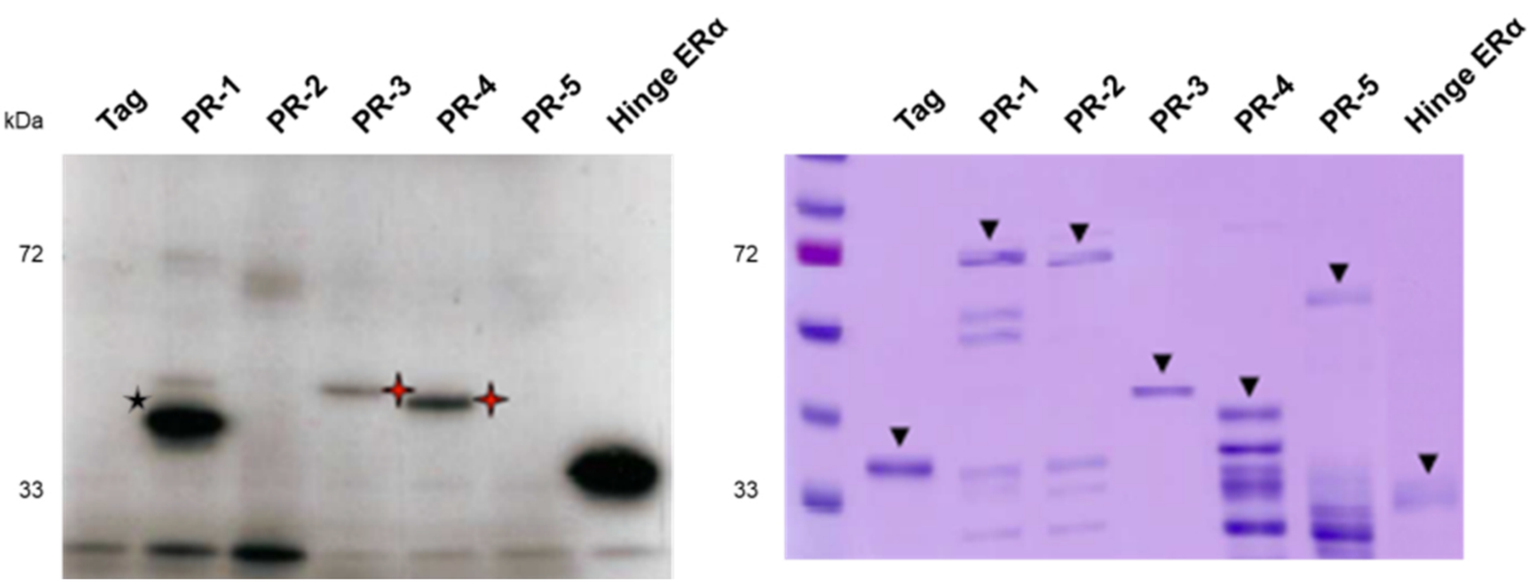
kDa
Tag
PR-1
PR-2
PR-3
PR-4
PR-5
Hinge ERα
72
33
Tag
PR-1
PR-2
PR-3
PR-4
PR-5
Hinge ERα
72
33

E.

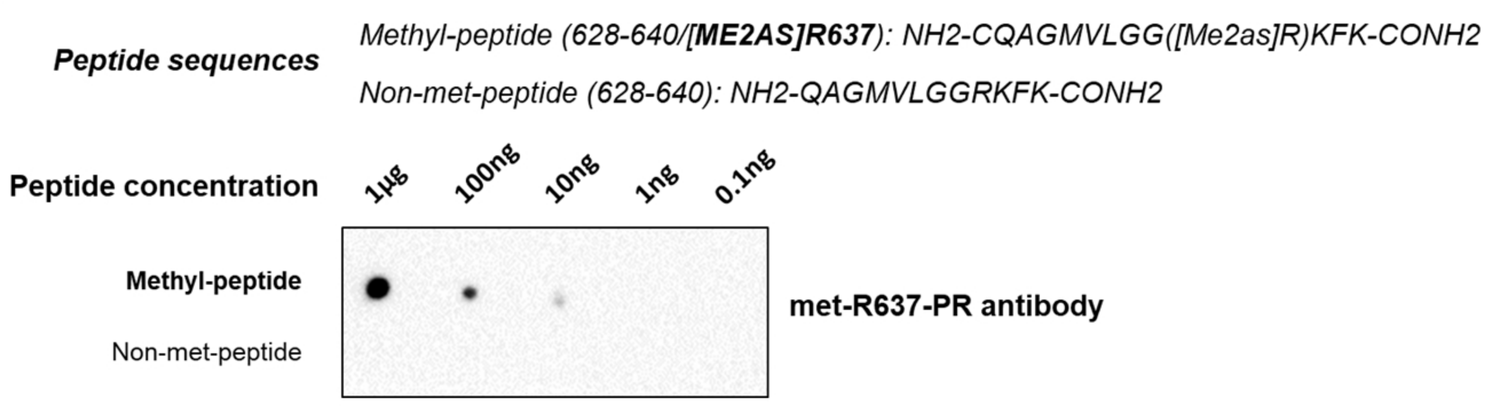
Peptide sequences
Methyl-peptide (628-640/[ME2AS]R637): NH2-CQAGMVLGG([Me2as]R)KFK-CONH2
Non-met-peptide (628-640): NH2-QAGMVLGGRKFK-CONH2
Peptide concentration
1μg
100ng
10ng
1ng
0.1ng
Methyl-peptide
Non-met-peptide
met-R637-PR antibody

F.

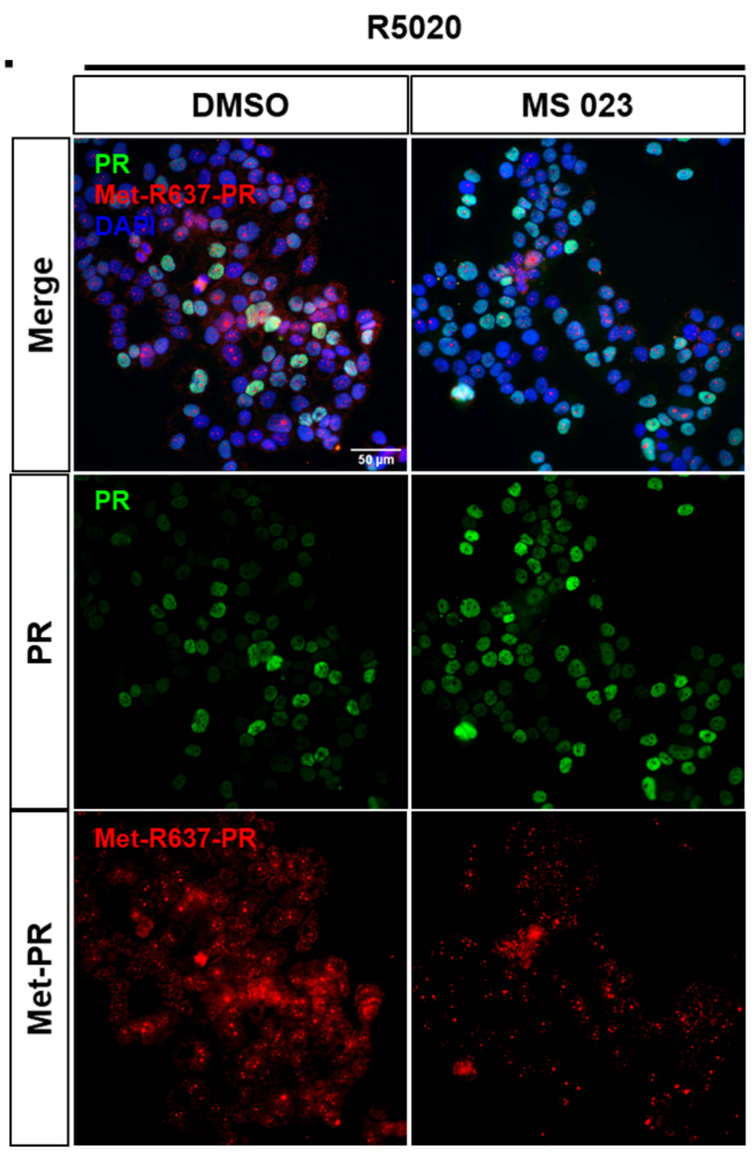
R5020
DMSO
MS 023
Merge
PR
Met-R637-PR
DAPI
50 μm
PR
PR
Met-R637-PR
Met-PR

Figure S2, related to Fig. 2 | PR is methylated on arginine residues in R5020-stimulated T47D breast cancer cells. A-B. Analysis of MS 023 inhibitor specificity. **A**. Immunoblot of R5020-stimulated T47D cells (1h), treated or not (DMSO) with different quantities of MS 023. Expression of indicated proteins were analyzed. **B.** Immunofluorescence of T47D cells, treated with 60 nM of MS 023 (or DMSO) and then stimulated 1h with 10 nM of R5020, using anti-H4R3me2(as) primary antibody. The nuclei were counterstained with DAPI (blue) (Obj: X40). **C.** Schematic representation of human GST-tagged PR fragments used for the *in vitro* methylation assays. **D.** An *in vitro* methylation assay was conducted by incubating different recombinant GST-PR fragments, GST-ER hinge used as a positive control and GST (tag) as a negative control, with recombinant GST-PRMT1, in the presence of [methyl-3H] SAM. Reaction products were analyzed by SDS-PAGE followed by fluorography. The migration and the quality of recombinant GST-fragments used as substrates were verified by a Coomassie-stained SDS-PAGE gel, shown in the right panel. The methylated proteins were visualized by autoradiography. Red stars indicate the methylated fragments of PR. Black star indicates a bacteria associated contaminant, as the signal did not correspond to any detectable fragment by Coomassie blue staining gel, shown in the right panel. **E.** Dot-blot was performed using increasing amounts of the indicated peptides, asymmetrically methylated or not on the arginine 637, and immunoblotted with the met-R637-PR antibody. Peptide sequences were shown in the upper panel. **F.** Immunofluorescence assay performed on T47D cells treated with 60 nM of MS 023 inhibitor (or DMSO) and stimulated with 10 nM of R5020 for 1h using the met-R637-PR and anti-PR antibodies. The nuclei were counterstained with DAPI (blue) (Obj: X40).

A.

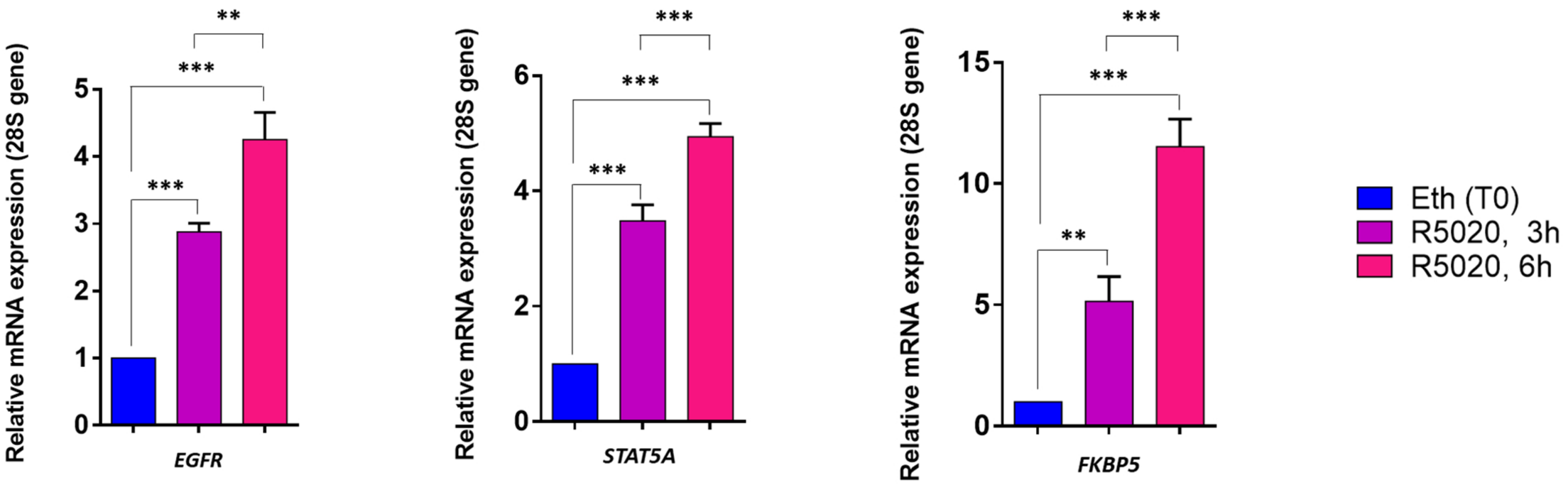

B. **ZR-75 cells**

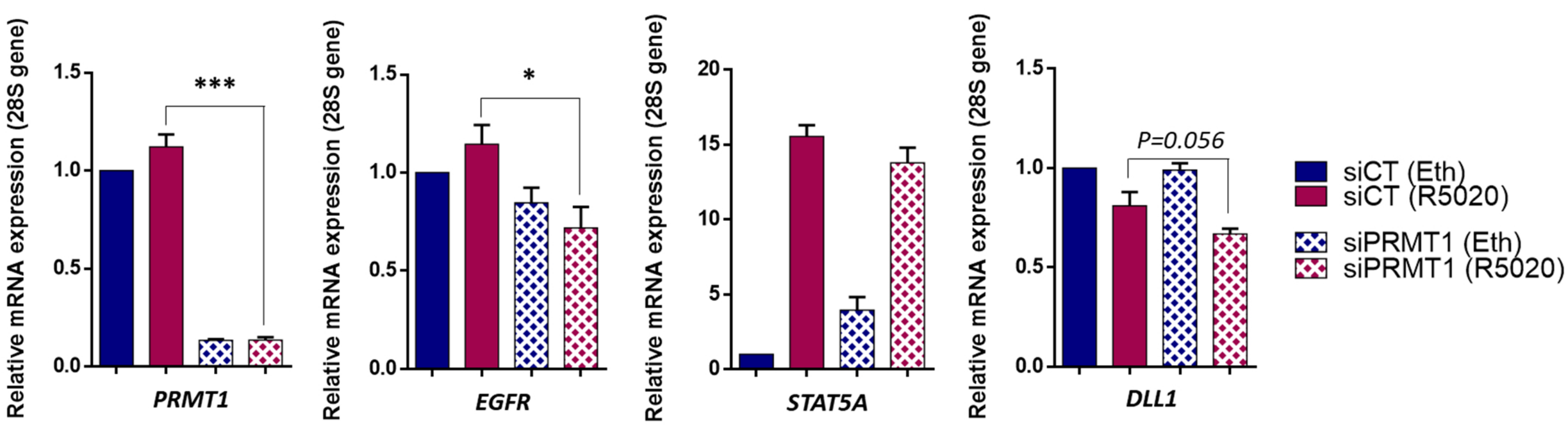

C. **T47D cells**

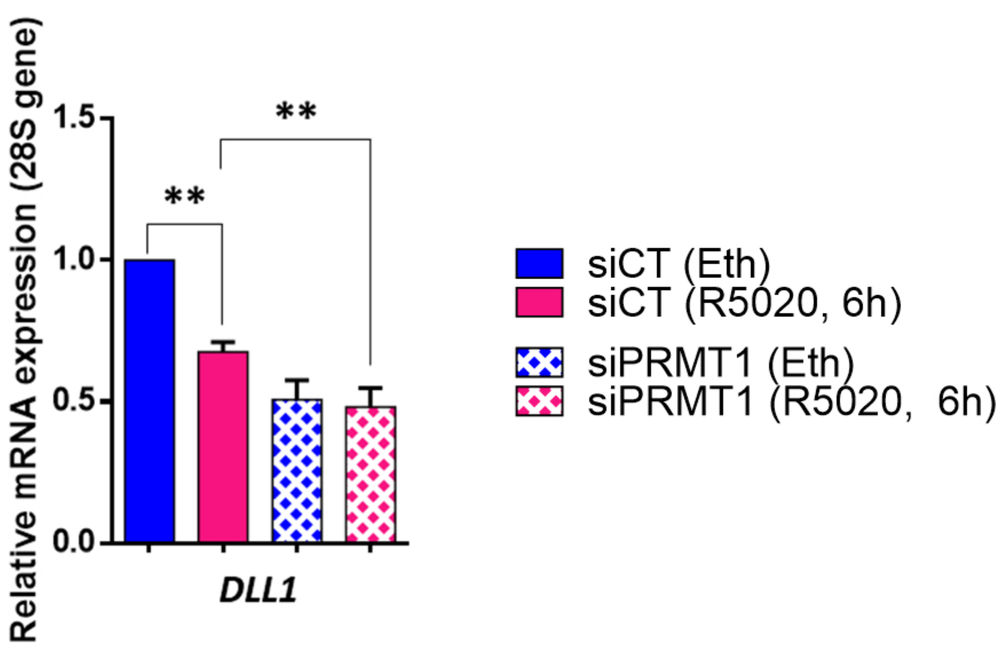

Figure S3, related to Fig. 4 | PRMT1 acts as a PR coregulator in breast cancer cells. A. RNAs were extracted for T47D cells, stimulated with R5020 for 3h or 6h (or with vehicle ethanol) and the expression of three endogenous PR-target genes was analyzed by RT-qPCR using specific primers. Results shown are mean ± SEM for three independent experiments. The *p*-value was calculated using a paired *t*-test: ** indicates $p \leq 0.01$ and ***$p \leq 0.001$. **B.** The expression of the indicated genes was analyzed by RT-qPCR using total RNA extracts from ZR-75 or **C.** T47D cells, previously transfected with siCT or siPRMT1 and stimulated with R5020 for 6h. The mean ± SEM of, at least, three independent experiments is shown. The *p*-value was calculated using a paired *t*-test: * indicates $p \leq 0.05$, ** $p \leq 0.01$ and *** $p \leq 0.001$.

A.

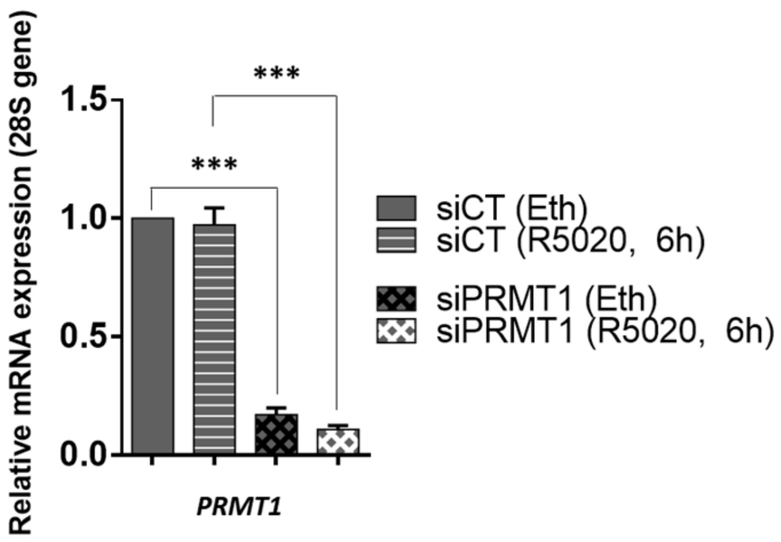
Relative mRNA expression (28S gene)
1.5
1.0
0.5
0.0
***
***
PRMT1
siCT (Eth)
siCT (R5020, 6h)
siPRMT1 (Eth)
siPRMT1 (R5020, 6h)

B.

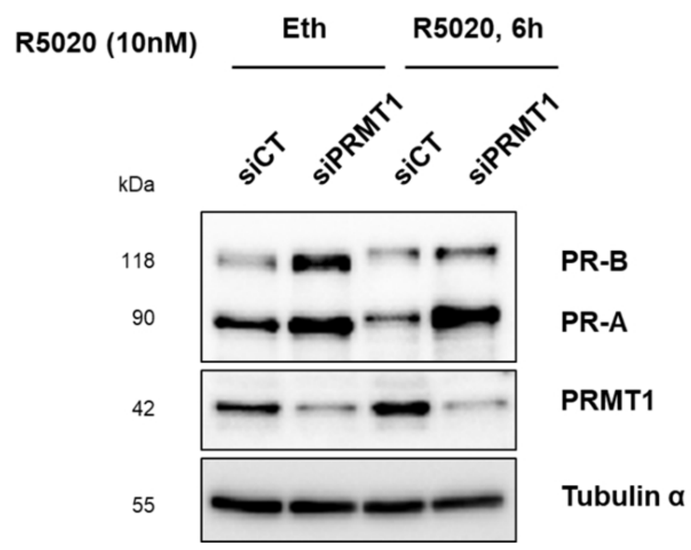
R5020 (10nM)
Eth
R5020, 6h
siCT
siPRMT1
siCT
siPRMT1
kDa
118
90
42
55
PR-B
PR-A
PRMT1
Tubulin α

C.

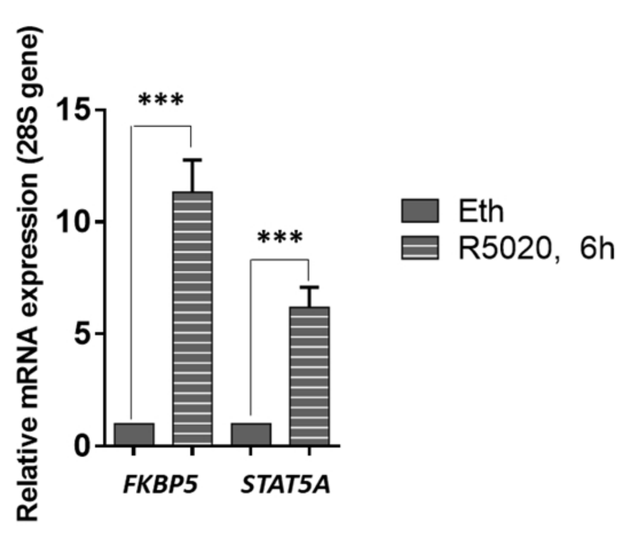
Relative mRNA expression (28S gene)
15
10
5
0
***
***
FKBP5
STAT5A
Eth
R5020, 6h

D.

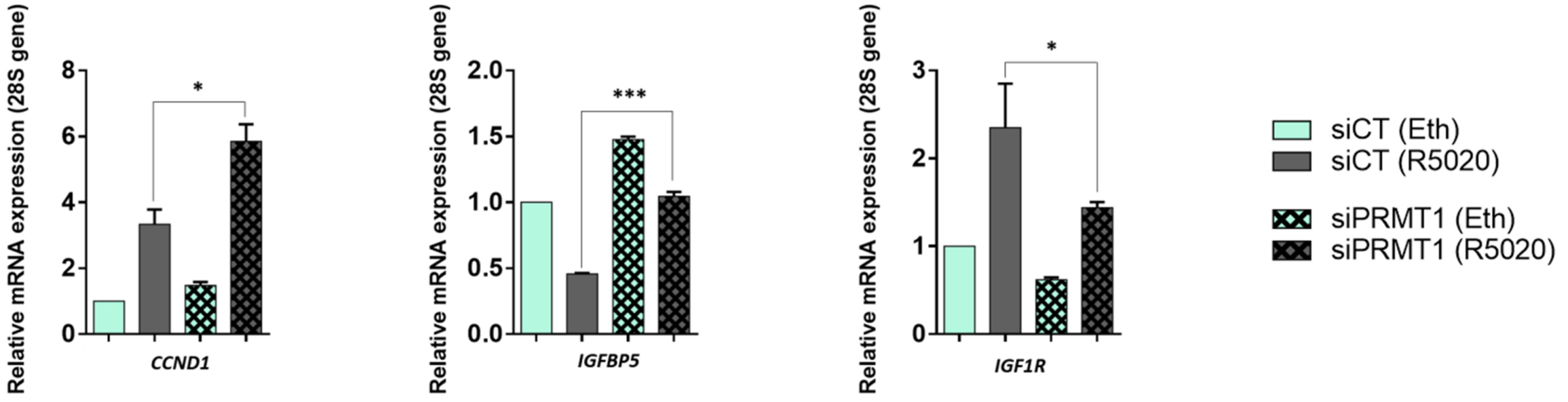
Relative mRNA expression (28S gene)
8
6
4
2
0
*
CCND1
2.0
1.5
1.0
0.5
0.0
***
IGFBP5
3
2
1
0
*
IGF1R
siCT (Eth)
siCT (R5020)
siPRMT1 (Eth)
siPRMT1 (R5020)

E.

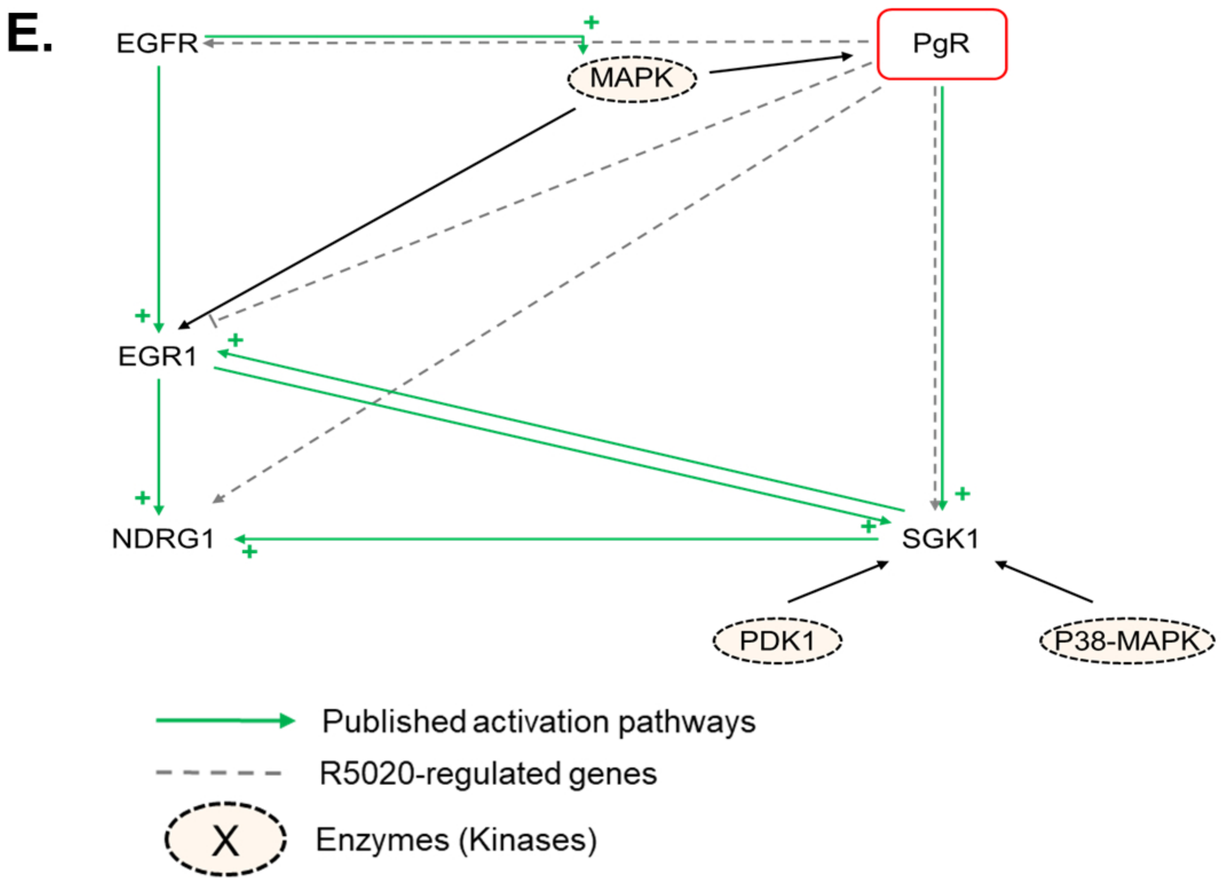
EGFR
PgR
MAPK
EGR1
NDRG1
SGK1
PDK1
P38-MAPK
Published activation pathways
R5020-regulated genes
X
Enzymes (Kinases)

F.

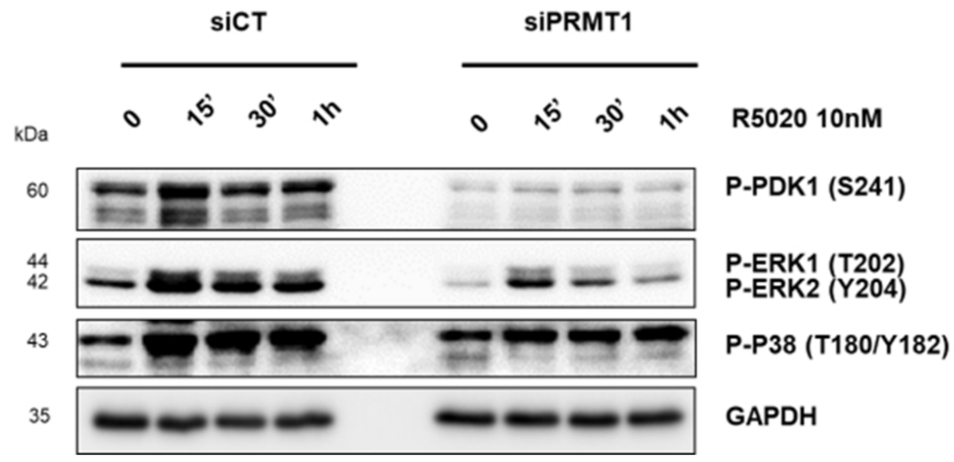
siCT
siPRMT1
0
15'
30'
1h
0
15'
30'
1h
R5020 10nM
kDa
60
44
42
43
35
P-PDK1 (S241)
P-ERK1 (T202)
P-ERK2 (Y204)
P-P38 (T180/Y182)
GAPDH

G.

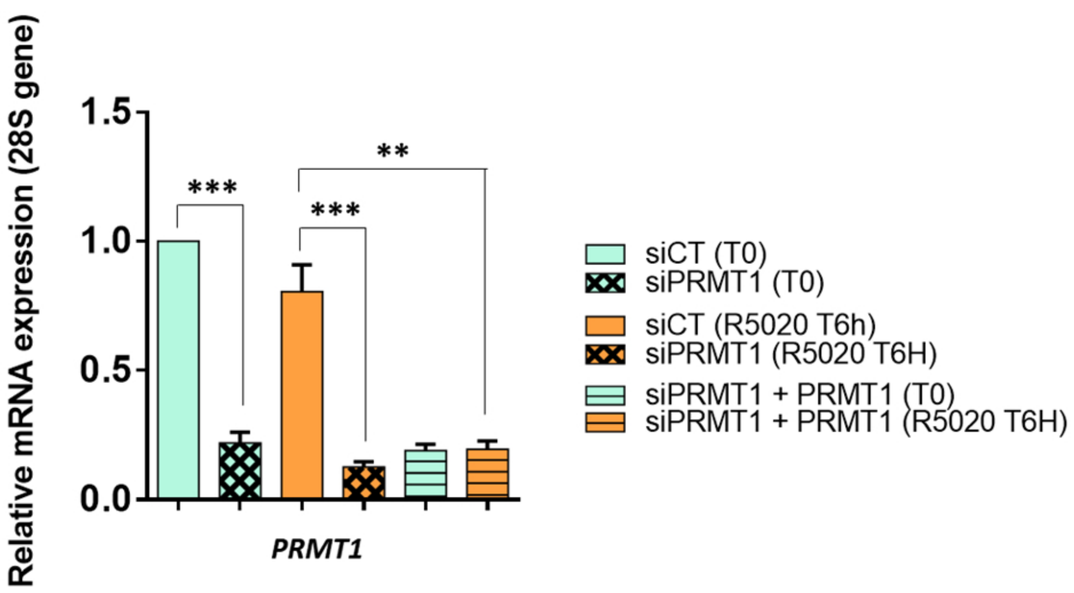
Relative mRNA expression (28S gene)
1.5
1.0
0.5
0.0
***
***
**
PRMT1
siCT (T0)
siPRMT1 (T0)
siCT (R5020 T6h)
siPRMT1 (R5020 T6H)
siPRMT1 + PRMT1 (T0)
siPRMT1 + PRMT1 (R5020 T6H)

H.

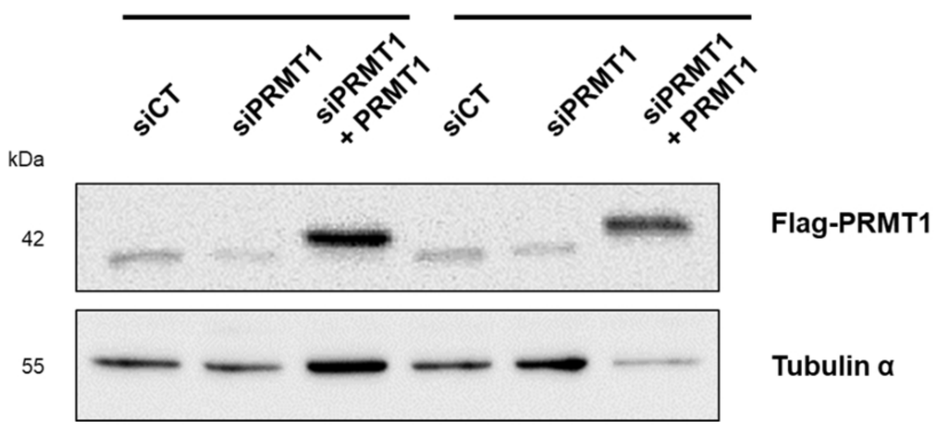
Eth
R5020 6h
siCT
siPRMT1
siPRMT1 + PRMT1
siCT
siPRMT1
siPRMT1 + PRMT1
kDa
42
55
Flag-PRMT1
Tubulin α

Figure S4, related to Fig. 5 | PRMT1 affects the expression of endogenous PR target genes in T47D cells. A-C. PRMT1 knockdown and hormonal treatment of T47D, stimulated for 6h of R5020 and used for RNA-seq analysis described in fig. 5. **A.** RT-qPCR analysis using *PRMT1* specific primers. **B**. Immunoblot using the indicated antibodies. **C.** RT-qPCR analysis using primers of *FKBP5* and *STAT5*, two well-characterized PR target genes. **D.** Genes randomly selected from the list of PRMT1-dependent genes identified by the RNA-seq analysis, were analyzed by RT-qPCR using total RNA extracts from T47D, transfected with either siCT or siPRMT1 and stimulated for 6h of R5020. The mean ± SEM of at least three independent experiments is shown. The *p*-value was calculated using a paired *t*-test: * indicates $p \leq 0.05$, ** $p \leq 0.01$ and *** $p \leq 0.001$. **E.** Scheme of the regulation of proteins involved in migration and proliferation pathways dependent on PR, according to the literature. **F.** Whole-cell extracts of T47D, depleted or not for PRMT1 using siRNA and treated with R5020 for the indicated times, were collected and subjected to immunoblot analysis using the listed antibodies. **G-H.** T47D cells were transfected with siRNAs (control or PRMT1) or co-transfected with siRNA plus a plasmid expressing the flag-tagged rat PRMT1 for 48h, and then treated with 10 nM of R5020 (6h). **G.** The expression of endogenous PRMT1 mRNA was analyzed by RT-qPCR using human *PRMT1* primers. Results shown are mean ± SEM for three independent experiments. The *p*-value was calculated using a paired *t*-test: ** indicates $p \leq 0.01$ and *** $p \leq 0.001$. **H.** The transfected rat PRMT1 was detected by immunoblot using anti-PRMT1 antibody.

A.

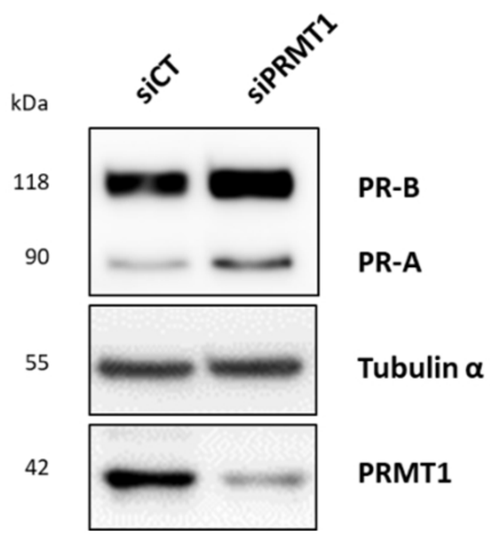

B. **Cell proliferation**

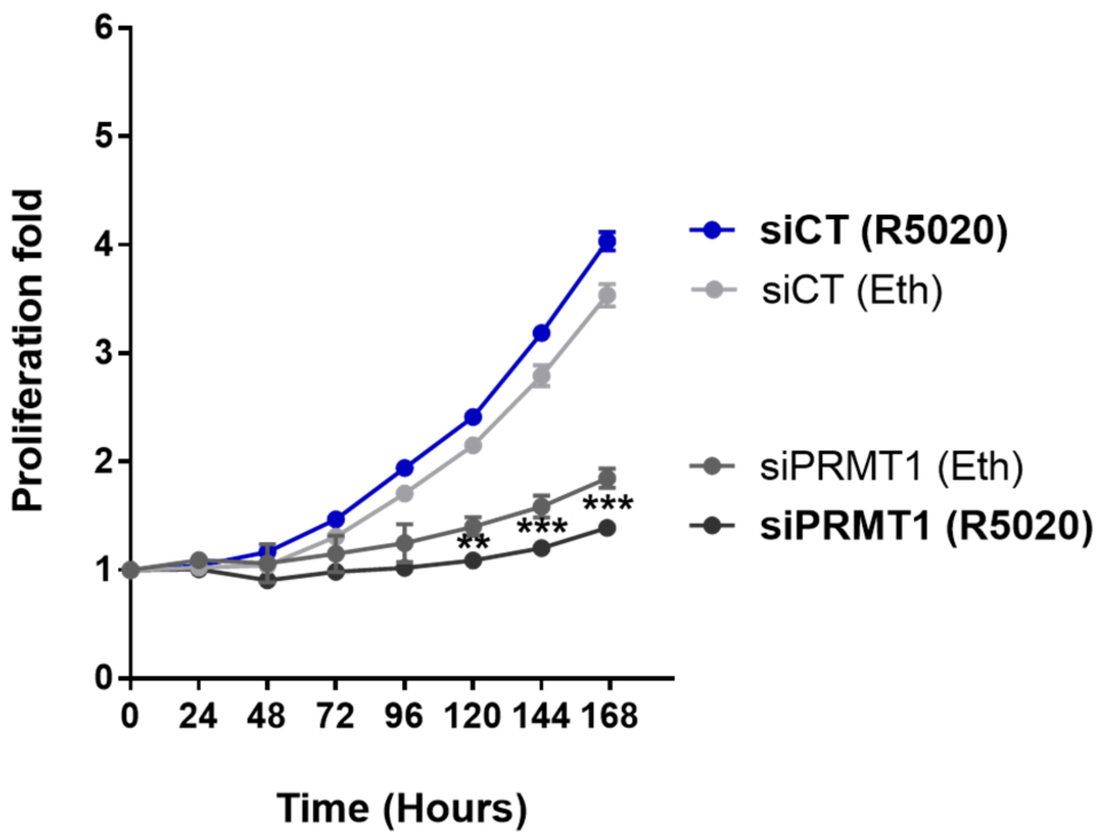

C. **Cell migration**

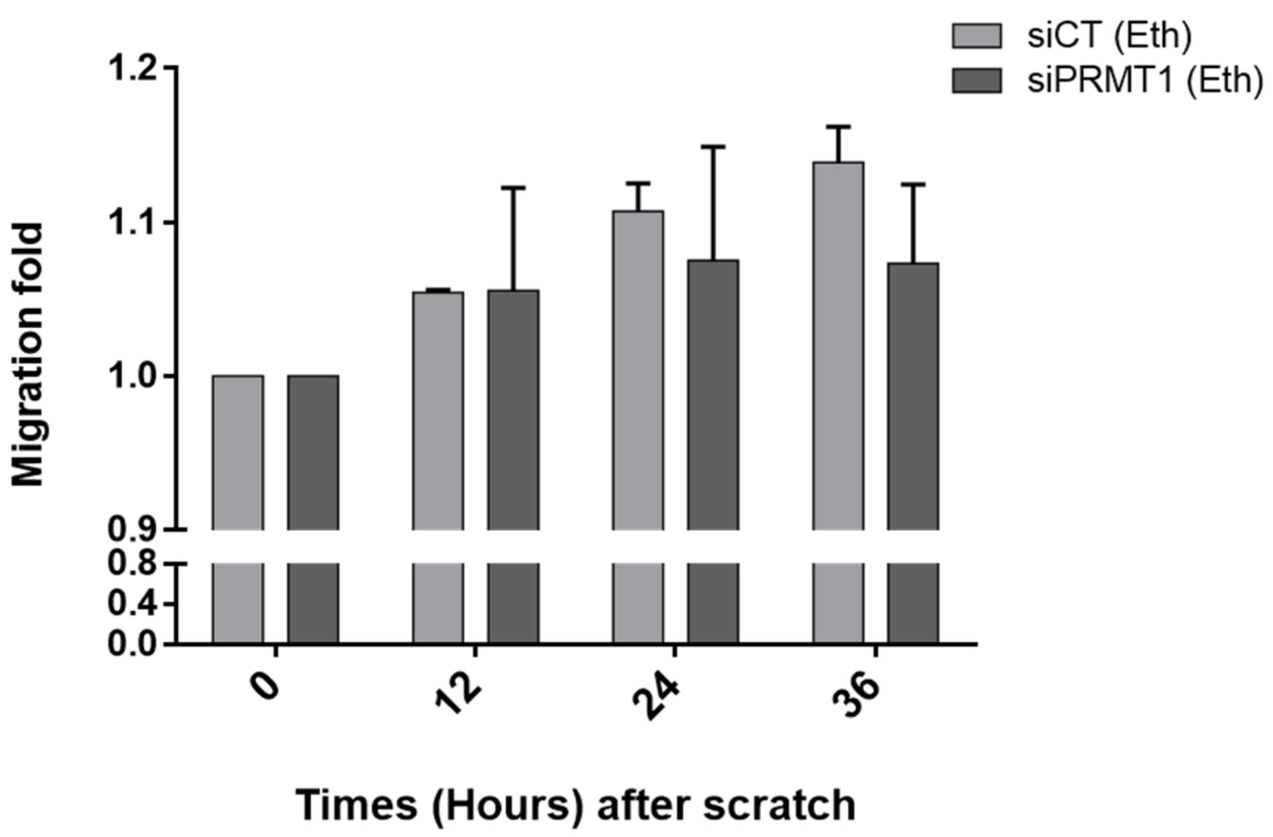

D.

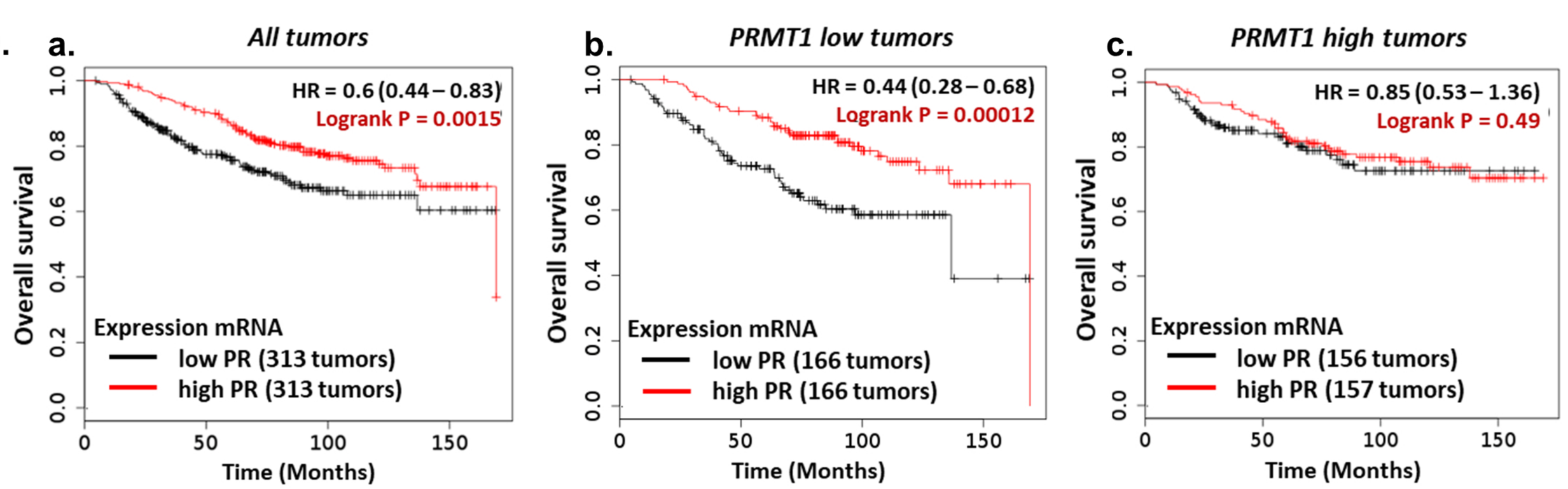

E.

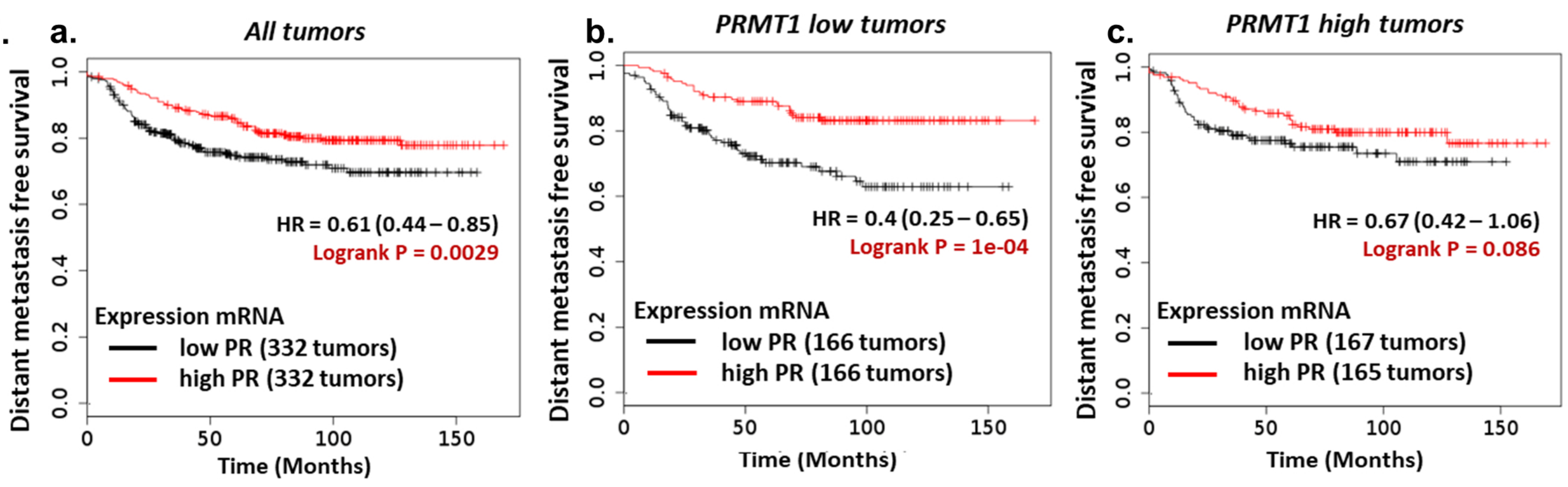

Figure S5, related to Fig. 6 | Low PRMT1 reduces R5020-induced proliferation and migration of T47D cells and predicts improved survival of breast cancer patients. A. T47D cells were transfected with siCT or siPRMT1 and used for proliferation and migration assays. Whole cell extracts were assessed for PRMT1 inhibition by IB. **B-C.** T47D cells expressing the indicated siRNAs (PRMT1 or CT) were analyzed by Incucyte technology. **B.** Cells were stimulated with R5020 (10 nM) or vehicle ethanol every 48h for 7 days and their proliferation rate was assessed. Image acquisition was conducted as explained in fig. 6B. **C.** T47D cells were kept unstimulated (vehicle ethanol) and their migration was analyzed in a wound scratch assay with the Incucyte Live-Cell Imaging System and dedicated software (Essen Bioscience), as reported in the Transparent Methods section. Both **B.** and **C.** graphs show the mean ± SD of one experiment representative of three. The *p*-value was determined using the Student's t-test: ** indicates $p \leq 0.01$ and *** $p \leq 0.001$. **D-E.** Kaplan-Meier estimates **D.** overall survival and **E.** distant metastasis free survival in patients, in GEO, EGA, TCGA datasets with low (black) or high (red) PR expression as indicated using KM-plotter in a cohort of 1764 breast tumors **(a)**, or stratified in 2 groups following low PRMT1 **(b)** or high PRMT1 expression **(c)**.

A.

T47D

Alignment result: (The first sequence is the reference sequence)

```
     1                                                                                                  100
1    ----------------------------------------------------------------------------------------------------  1

1    CCCTCCCGCCTGCGAGGTCACCAGCTCTTGGTGCCTGTTTGGCCCCGAACTTCCCGAAGATCCACCGGCTGCCCCCGCCACCCAGCGGGTGTTGTCCCCG 100

   101                                                                                                  200
1    ----------------------------GAGACAGCTCCGGGACGGCAGCTGCCCATAAAGTGCTGCCCCGGGGCCTGTCACCAGCCCGGCAGCTGCTGC  72
                                 ||||||||||||||||||||||||||||||||||||||||||||||||||||||||||||||||||||||||
101  CTCATGAGCCGGTCCGGGTGCAAGGTTGGAGACAGCTCCGGGACGGCAGCTGCCCATAAAGTGCTGCCCCGGGGCCTGTCACCAGCCCGGCAGCTGCTGC 200

   201                                                                                                  300
73   TCCCGGCCTCTGAGAGCCCTCACTGGTCCGGGGCCCCAGTGAAGCCGTCTCCGCAGGCCGCTGCGGTGGAGGTTGAGGAGGAGGATGGCTCTGAGTCCGA 172
     ||||||||||||||||||||||||||||||||||||||||||||||||||||||||||||||||||||||||||||||||||||||||||||||||||||
201  TCCCGGCCTCTGAGAGCCCTCACTGGTCCGGGGCCCCAGTGAAGCCGTCTCCGCAGGCCGCTGCGGTGGAGGTTGAGGAGGAGGATGGCTCTGAGTCCGA 300
```

Clone #2

Alignment result: (The first sequence is the reference sequence)

```
     1                                                                                                  100
1    GAGACAGCTCCGGGACGGCAGCTGCCCATAAAGTGCTGCCCCGGGGCCTGTCACCAGCCCGGCAGCTGCTGCTCCCGGCCTCTGAGAGCCCTCACTGGTC 100
1    ----------------------CTGCCCATAAAGTGCTGCCCCGGGGCCTGTCACCAGCCCGGCAGCTGCTGCTCCCGGCCTCTGAGAGCCCTCACTGGTC  79
1    ----------------------CTGCCCATAAAGTGCTGCCCCGGGGCCTGTCACCAGCCCGGCAGCTGCTGCTCCCGGCCTCTGAGAGCCCTCACTGGTC  79

     101                                                                                                200
101  CGGGGCCCCAGTGAAGCCGTCTCCGCAGGCCGCTGCGGTGGAGGTTGAGGAGGAGGATGGCTCTGAGTCCGAGGAGTCTGCGGGTCCGCTTC-TGAAGGG 199
80   CGGGGCCCCAGTGAAGCCGTCTCCGCAGGCCGCTGCGGTGGAGGTTGAGGAGGAGGATGGCTCTGAGTCCGAGGAGTCTGCGGGTCCGCTTC-TGAAGGG 178
80   CGGGGCCCCAGTGAAGCCGTCTCCGCAGGCCGCTGCGGTGGAGGTTGAGGAGGAGGATGGCTCTGAGTCCGAGGAGTCTGCGGGTCCGCTTCTTGAAGGG 179

     201                                                                                                300
200  CAAACCTCGGGCTCTGGGTGGCGCGGCGGCTGGAGGAGGAGCCGCGGCTGTCCCGCCGGGGGCGGCAGCAGGAGGCGTCGC------------------- 280
179  CAAACCTCGGGCTCTGGGTGGCGCGGCGGCTGGAGGAGGAGCCGCGGCTGTCCCGCCGGGGGCGGCAGCAGGAGGCGTCGCCCTGGTCCCCAAGGAAGAA 278
180  CAAACCTCGGGCTCTGGGTGGCGCGGCGGCTGGAGGAGGAGCCGCGGCTGTCCCGCCGGGGGCGGCAGCAGGAGGCGTCGCCCTGGTCCCCAAGGAAGTT 279
```

Clone #3

Alignment result: (The first sequence is the reference sequence)

```
     1                                                                                                  100
1    GAGACAGCTCCGGGACGGCAGCTGCCCATAAAGTGCTGCCCCGGGGCCTGTCACCAGCCCGGCAGCTGCTGCTCCCGGCCTCTGAGAGCCCTCACTGGTC 100
1    G----------------GCAGCTGCCCATAAAGTGCTGCCCCGGGGCCTGTCACCAGCCCGGCAGCTGCTGCTCCCGGCCTCTGAGAGCCCTCACTGGTC  84
1    G----------------GCAGCTGCCCATAAAGTGCTGCCCCGGGGCCTGTCACCAGCCCGGCAGCTGCTGCTCCCGGCCTCTGAGAGCCCTCACTGGTC  84

     101                                                                                                200
101  CGGGGCCCCAGTGAAGCCGTCTC-CGCAGGCCGCTGCGGTGGAGGTTGAGGAGGAGGATGGCTCTGAGTCCGAGGAGTCTGCGGGTCCGCTTCTGAAGGG 199
85   CGGGGCCCCAGTGAAGCCGTCTC--GCAGGCCGCTGCGGTGGAGGTTGAGGAGGAGGATGGCTCTGAGTCCGAGGAGTCTGCGGGTCCGCTTCTGAAGGG 182
85   CGGGGCCCCAGTGAAGCCGTCTCACGCAGGCCGCTGCGGTGGAGGTTGAGGAGGAGGATGGCTCTGAGTCCGAGGAGTCTGCGGGTCCGCTTCTGAAGGG 184

     201                                                                                                300
200  CAAACCTCGGGCTCTGGGTGGCGCGGCGGCTGGAGGAGGAGCCGCGGCTGTCCCGCCGGGGGCGGCAGCAGGAGGCGTCGC------------------- 280
183  CAAACCTCGGGCTCTGGGTGGCGCGGCGGCTGGAGGAGGAGCCGCGGCTGTCCCGCCGGGGGCGGCAGCAGGAGGCGTCGCCCCGTGGTCCCCAGGGAAT 282
185  CAAACCTCGGGCTCTGGGTGGCGCGGCGGCTGGAGGAGGAGCCGCGGCTGTCCCGCCGGGGGCGGCAGCAGGAGGCGTCGCTCGG----CCCCAAGAAAG 280
```

B.

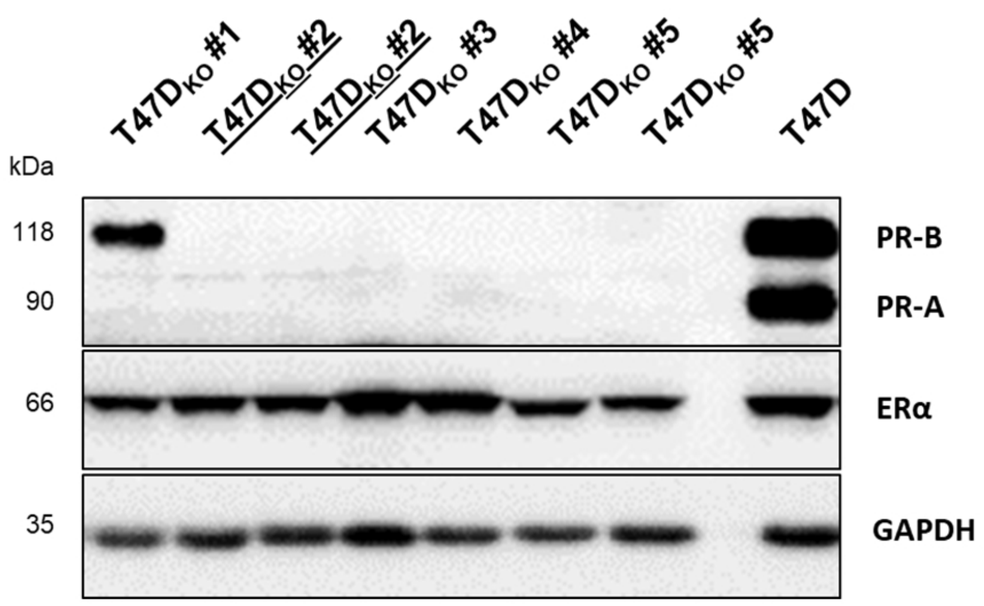

C.

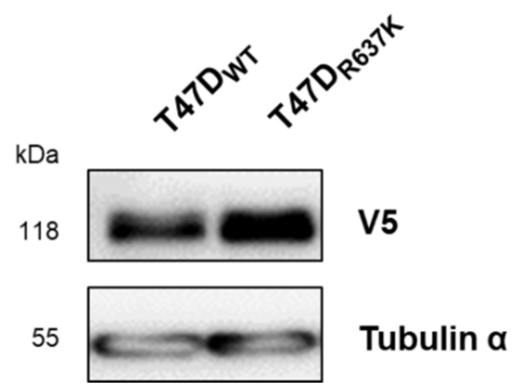

Figure S6, related to Fig. 7 | Inhibiting PR methylation decreases breast cancer cell proliferation and PR turnover. A. Chromatograms showing DNA sequences from mock and CRISPR-Cas9 cells. We performed genotyping PCRs. The amplified fragments were sequenced using an oligo targeting a sequence inside the fragment and analyzed using CRISP-ID, a web application. This tool allows the detection of the exact indel size and the location of a CRISPR-Cas9 targeted region, based on direct Sanger sequencing (as described in the Transparent Methods section). **B.** Whole-cell extracts of different clones of T47D PR_{KO} were collected and analyzed by immunoblot for their expression of PR, using PR-antibody, as well as ERα. The clone #2 (underlined) was chosen for stably re-expressing PR_{WT} or PR_{R637K}, as observed in experiences of fig. 7. T47D (PR-positive) cell line was used as control. **C.** Cell lysates of PR_{WT} and PR_{R637K}, used for cell proliferation test shown in fig. 7E and for the colony growth assay (fig. 7F), were collected and analyzed by immunoblot for their expression of PR-V5.

Transparent Methods

Cell culture and treatments

T47D (ATCC) were cultured in RPMI-1640 medium, supplemented with 10% fetal bovine serum (FBS), 2% penicillin-streptomycin (Life Technologies) and insulin (10 µg/ml). Cos7 and HeLa cells (ATCC) were maintained in DMEM, supplemented with 10% FBS and 2% penicillin-streptomycin (Life Technologies). All cell lines were grown in a humidified atmosphere with 5% CO_2 at 37°C, authenticated by Eurofins and tested for Mycoplasma infection by the MycoAlert Mycoplasma Detection Assay (Lonza, Rockland, ME USA).

Prior to experiments, T47D cells were grown in phenol red-free medium supplemented with 10% charcoal-stripped serum (Biowest). 48h later, medium was replaced by fresh serum-free medium. After 48h in serum-free conditions, cells were treated with 10 nM of R5020 (Perkin Elmer) or an equivalent amount of ethanol vehicle for the indicated time. When indicated, inhibitors (or DMSO vehicle) were added to cells: MS 023 Type I PRMT inhibitor (Tocris) for 48h, at the indicated concentration, cyclohemixide (Sigma, 50 µM) or MG132 proteasome inhibitor (Sigma, 10 µM) for 16h or 8h respectively, before R5020 treatment.

Plasmids and constructions

The GST-PR vectors (GST-PR-1, -PR-2, -PR-3, -PR-4, -PR-5 and -PR-3-R637A mutant) were constructed by inserting the cDNA fragments illustrated in Figure S2C, obtained by PCR amplification, into the pET41a vector (Novagen). All of the PR mutants were generated using a QuikChange XL Site-Directed Mutagenesis kit (Stratagene) according to the manufacturer's instructions and the sequences were verified by DNA sequencing. The mammalian expression vector pSG5-PR(B) was a gift from Pr. P. Chambon (Kastner et al., 1990). pSG5V5-PR(B) was obtained by inserting the V5-TAG coding sequence in frame with the coding sequence of PR(B) by PCR.

pSG5V5-PR(B) plasmid was used to generate PR-R637A. To rescue the phenotype of PR_{KO} clones, a guide-resistant mutant of the PR(B) isoform was created (pSG5V5gr) by substituting four nucleotides in the PR guide 1 (G633A, G6364, T639C and G641A) and four nucleotides in the PR guide 2 (C715T, T717A, C718T and G720A) targeting regions. This guide-resistant PR(B) was cloned into the stable mammalian expression vector pPRUpu. pSG5V5gr PR(B) and pPRUpuV5gr-PR(B) were used to obtain the PR-R637K. Sequences of the primers used for the constructions are listed in Table S2. The human HA-PRMT1 and HA-PRMT1(E153Q) in pSG5 vector were a gift of C. Teyssier (Teyssier et al., 2005) and the rat flag-PRMT1 in pSG5 vector was previously described (Robin-Lespinasse et al., 2007).

Generation of CRISPR cell lines: PR_{KO}

To knockout PR genes in T47D cells, we used the pLCV2 plasmid (a gift from F. Zhang, Addgene plasmid #52961). Oligonucleotides pairs were hybridized and cloned into the LentiCRISPR V2 vector linearized with BsmB1 to generate T47D clones KO: PR Guide#1 – Fwd. CACCGcccagtgaagccgtctccgc / Rev. AAACgcggagacggcttcactgggC; PR Guide #2 – Fwd. CACCGtctgcgggtccgcttctgaa / Rev. AAACttcagaagcggacccgcagaC, oligonucleotides targeting the regions 624-637 and 693-713 of the PR(B) coding sequence. T47D cells were transfected with the corresponding LentiCRISPR V2 plasmids and selected with blasticidin (5 μg/ml, Invitrogen, Grand Island, NY, USA) for 1 week. Cells were then cloned in 96-well plates by limiting dilution. Isolated clones were characterized by immunoblotting. For five different clones, we confirmed the knockout at DNA and protein levels. We performed genotyping PCRs using a forward primer upstream (5'-GGGGAGTCCAGTCGTCAT-3') and a reverse primer downstream (5'-ACTTTCGTCTTCCAGCAGC-3') of the sgRNA cleavage site. The amplified fragments were then sequenced using an oligo targeting a sequence inside the fragment (5'-CCAGAAAAGGACAGCGGAC-3') and analyzed using CRISP-ID, a web application that allows the detection of the exact indel size and location of a CRISPR-Cas9 targeted region, based on direct Sanger sequencing (Dehairs et al., 2016).

Generation of two stable cell lines: $T47D_{WT}$ and $T47D_{R637K}$

For the production of the rescue cell lines, CRISPR PR_{KO} cells were transfected with pPRUpuPR(B)-WT and -R637K plasmids using Jetprime (Polyplus-transfection). Screening of stable transfected cells was performed using puromycin dihydrochloride, 1 µg/ml. Stable cell populations, called $T47D_{WT}$ and $T47D_{R637K}$, were maintained in complete RPMI-1640 medium containing 0.5 µg/ml of puromycin.

Generation of methylated-R637-PR antibody (anti-met-R637-PR)

Rabbits were immunized with a peptide corresponding to PR amino acids 628-640 (NH2-CQAGMVLGG([Me2as]R)KFK-CONH2), in which R637 was asymmetrically dimethylated by Covalab (Villeurbanne, France). To purify the met-R637-PR antibody, the dimethyl peptide used for the immunization and the corresponding control peptide (non-methyl) were coupled separately to cyanogen bromide activated agarose beads. The antisera were first bound on the non-methylated peptide column. The unbound antiserum was then applied to the methylated peptide column and eluted. The title and the specificity of the purified antibody were then tested by enzyme-linked immunosorbent assay (ELISA).

Glutathione transferase (GST) pull-down assay

The GST-PRMT1 and GST-PR fusion proteins were expressed in BL21 competent cells and purified using glutathione-sepharose 4B resin (GE Healthcare Life Sciences). SDS-PAGE and Coomassie staining were used to confirm the integrity of the fusion proteins. PR-B or ERα expression plasmids were transcribed and translated *in vitro* using T7-coupled reticulocyte lysate in the presence of [^{35}S] methionine. For *in vitro* protein-protein interaction assays, GST fusion proteins were incubated for 2h at room temperature with 200 µl of binding buffer (Tris 20 mM pH 7.4, NaCl 0.1 M, EDTA 1 mM, glycerol 10%, Igepal 0.25% with 1 mM dithiothreitol and 1% milk) and packed in minicolumns. After washing, the retained proteins were eluted and analyzed on a sodium dodecyl sulfate (SDS) polyacrylamide gel electrophoresis (PAGE) and visualized by autoradiography.

In vitro methylation assays

GST-PRMT1 (Upstate Biotechnology) was incubated with different GST-tagged PR fragments, or with a GST-tagged hinge ERα as a positive control (Le Romancer et al., 2008), in the presence of S-adenosyl-l [methyl-^{3}H] methionine ([^{3}H] SAM 85 Ci/mmol from a 10.4 mM stock solution in dilute HCl/ethanol 9/1 (pH 2.0–2.5); Perkin Elmer) for 90 min at 37°C. Methylation reactions were quenched by the addition of 2x Laemmli sample buffer, heated at 95°C for 5 min and separated on SDS-PAGE. Following electrophoresis, gels were soaked in Amplify fluorographic reagent (Sigma) according to the manufacturer's instructions and visualized by autoradiography. The cold methylation assays were performed in the same experimental conditions, using 0.5 mM of nonradiolabeled AdoMet (SAM). The reaction mixtures were subjected to SDS-PAGE and then analyzed by western blot using the anti-met-R637-PR (homemade) antibody.

Dot immunoblot assay

A peptide corresponding to PR amino acids 628-640 (NH2-CQAGMVLGG([Me2as]R)KFK-CONH2), in which R637 was asymmetrically dimethylated, and the corresponding control peptide (non-methyl), were produced by Covalab (Villeurbanne, France). For dot blot assays, peptides were spotted onto nitrocellulose membrane allowing solution to penetrate (usually 3–4 mm diameter) by applying it slowly as a volume of 1 µL. The membrane was dried and analyzed by immunoblot using the anti-met-R637-PR (homemade) antibody.

siRNA and plasmid transfection

siRNA transfections were performed using Lipofectamine 2000 (Invitrogen, Thermofisher) according to the manufacturer's protocol. After 72h, the down-regulation was analyzed by immunoblot or by RT-qPCR. If requested, after 48h the medium was replaced by fresh medium without serum and cells were treated with R5020 (10 nM) or ethanol for different times.

Plasmid transfections were done using the JetPRIME reagent (Ozyme) according to the manufacturer's protocol. Cells were analyzed after the indicated times (48h or 72h). SiRNAs pool against PR, PRMT1, PRMT4 and PRMT6 were purchased from Thermofischer Scientific (catalog #AM16708) and the siRNA negative control from Eurogentec (catalog # SR-CL000-00). For the rescue experiments, the plasmid expressing rat-PRMT1 was co-transfected with siRNAs pool against PRMT1 using the JetPRIME reagent (Ozyme) according to the manufacturer's protocol.

Luciferase reporter assay

HeLa cells were plated in 96-well plates the day before transfection. Cells were transfected using Lipofectamine 2000 (Invitrogen) with the indicated plasmids according to the manufacturer's protocol. After transfection, the cells were grown for 48h in the presence or absence of 10 nM of R5020. Cell lysis and luciferase assays were performed with Promega luciferase assay kit. The results were normalized as indicated and presented as the mean ± SEM of three independent experiments.

Immunoprecipitation (IP), immunoblot (IB) and antibodies

After treatment, cells were lysed with RIPA buffer (50 mM Tris HCl pH 8, 150 mM NaCl, 1 mM ethylenediamine tetra-acetic acid (EDTA), 1% NP-40 and 0.25% deoxycholate) supplemented with protease inhibitors (Roche Molecular Biochemicals) and phosphatase inhibitors (1 mM sodium fluoride, 1 mM Na3VO4 and 1 mM β-glycerophosphate). For immunoprecipitation (IP), 1mg of protein extracts were incubated with primary antibodies at 4°C overnight. Protein A-Agorase beads were added in the medium for 2h at 4°C on a rotating wheel. After washing, the immunoprecipitates and their corresponding inputs (30µg) were denatured by boiling in Laemmli sample buffer and separated on SDS-PAGE. For immunoblot (IB), the gels were electroblotted onto a PVDF membrane and incubated with primary antibodies overnight, at 4°C. The following day, membranes were incubated with horseradish peroxidase (HRP)-conjugated anti-rabbit or anti-mouse immunoglobulins (Jackson Immunoresearch) and proteins were visualized by chemiluminescence (Clarity Western ECL Substrate,

BioRad) following the manufacturer's instructions. Quantification of the immunoblot band intensity was performed with Image J software. The primary antibodies used in the study, and their dilutions, are listed in Table S3.

Cycloheximide chase assay

$3x10^5$ cells were grown in complete RPMI medium for 24h and then in phenol red-free medium supplemented with 10% charcoal-stripped serum for 48h. 16h before starting the R5020 stimulation, 50 µg/mL cycloheximide (Sigma) or vehicle DMSO were added. After each R5020-time point, cells were lysed with protein lysis buffer with freshly-added protease inhibitors and analyzed by IB.

Immunofluorescence (IF)

T47D cells ($3x10^5$) and $T47D_{WT}$ or $T47D_{R637K}$ stable cells ($2x10^5$) were grown on coverslips in 12-well plates. After chemical treatment(s), cells were fixed in methanol for 2 min and washed twice in PBS. Non-specific binding was blocked using a 1% gelatin solution for 30 min at room temperature. Cells were incubated with the different primary antibodies (listed in Table S3) for 1h at 37°C and then with the secondary antibodies [Alexa Fluor 488 anti-mouse (Jackson ImmunoResearch, Cambridge, UK) ($1/2000^e$) or Alexa Fluor 568 anti-rabbit (Invitrogen, Carlsbard, USA) ($1/1000^e$)] in Dako diluent for 1h. To finish, coverslips were mounted on glass slides in mounting solution (Dako, Carpinteria, CA, USA). The fluorescent slides were viewed with the Nikon Eclipse Ni microscope.

Proximity ligation assays (PLA), image acquisition and analysis

PLA assays were performed to visualize protein/protein interactions *in situ*, using the Duolink kit (Sigma) according to the manufacturer's instructions. Cells ($3x10^5$) were grown on coverslips in 12-well plates and treated (as explained in figures and legends), before fixation with methanol for 2 min. After saturation in the blocking solution, seeded cells were incubated with different pairs of primary antibodies at 37°C for 1h. The PLA probes consisting of secondary antibodies conjugated with

complementary oligonucleotides were then incubated for the same conditions. The step of nucleotides ligation (30 min at 37°C) is followed by the amplification phase, for 100 min at 37°C in a dark and humidified chamber. At the end, coverslips were mounted on glass slides in mounting solution (Dako, Carpinteria, CA, USA) and were analyzed under fluorescence microscopy on a Nikon Eclipse Ni microscope. Images were acquired under identical conditions at 60X magnification. Image acquisition was performed by imaging DAPI staining at a fixed Z-Position, while a Z-stack of ± 5 µm at 1 µm intervals was carried out. The final image was stacked to a single level before further quantification. On each sample, at least one hundred cells were counted. Analysis and quantifications of these samples were performed using the Image J software (Version 1.52, NIH, Bethesda, MD, USA). The primary antibodies used in the study, and their dilutions, are listed in Table S3.

RNA extraction and real-time qPCR analysis

Total RNA (1 µg) was extracted and purified using TRI-Reagent (Sigma-Aldrich, USA), prior to being reverse-transcribed using 100 ng of random primers following the Superscript II (ThermoFisher, USA) protocol. Real time PCR was performed with SYBR Green qPCR master mix (BioRad) in a Step One plus real-time PCR detection system (Applied Biosystems). Mean values of measurements were calculated according to the -ΔΔCt quantification method and were normalized against the expression of 28S ribosomal mRNA as reference. Results shown are mean ± SEM for, at least, three independent experiments. The *p*-value was calculated using a paired *t*-test comparing results for R5020-treated cells expressing siRNA against PRMT1 to the R5020-treated siCT sample: * indicates a $p \leq 0.05$, ** for $p \leq 0.01$ and *** for $p \leq 0.001$. Sequences of the oligonucleotides are listed in Table S4.

Chromatin ImmunoPrecipitation (ChIP)

Chromatin was prepared from 5x106 of T47D cells (untreated or treated with 10 nM of R5020 for 1h). Cells were crosslinked with 1% formaldehyde (Sigma-Aldrich, USA) for 10 min at room temperature and then treated with 0.125 M glycine for 5 min under a gentle shaking. Nuclei were lysed in 300 µL of

ice-cold RIPA buffer (50 mM Tris HCl pH 8, 150 mM NaCl, 1% NP-40, 0.5% NaDoc and 0.1% SDS) prior to Chromatin-DNA shearing with a Diogene Bioruptor. ChIP was performed with the primary antibodies listed in Table S3. The antibody–chromatin complexes were precipitated with salmon sperm DNA/protein A agarose beads for 3h by rotation. Samples were extracted and heated at 65°C for 5h to reverse cross-links. After DNA purification, 2 ng of input DNA were used for qPCR analysis to quantify co-precipitated chromatin-DNA. Relative enrichment of a given promoter region obtained with a specific antibody was compared with Input DNA, normalized to a reference locus (human chromosome 1 in which no histone modification was reported). Sequences of the primers used to amplify ChIP-enriched DNA are listed in Table S4.

RNA-sequencing and RNA-seq analysis

RNA-Sequencing experiment was performed using T47D cells. Cells were transfected with siCT or siPRMT1 (50 nM) for 72h and treated with R5020 (10 nM) for 6h before RNA extraction. Sequencing was done by the IGFL (Institute of Functional Genomic of Lyon) Sequencing Platform, to compare gene expression levels of R5020-induced genes between siCT and siPRMT1 conditions. cDNA libraries were prepared using the SENSE mRNA-Seq Library Prep Kit V2 (Lexogen, Vienna Austria). Quality of the cDNA was assessed and RT-qPCR was performed for selected PR target genes as quality control. All libraries were sequenced on an Illumina Nextseq500 and mapped on the hg19 version of the human genome using Bowtie2 (Galaxy Version 2.3.2.2). Count tables were prepared using htseq-count (Galaxy Version 0.9.1galaxy3). Differential gene expression analysis was performed with DEseq2 (Galaxy Version 2.1.8.3) using different thresholds. For R5020-induced genes in siCT-cells: FDR < 0.05; *p*-adjusted value < 0.01; fold-change > 2; expression > 10 reads per million. For R5020-induced genes in siPRMT1-cells: FDR < 0.05; *p*-adjusted value < 0.01; fold-change > 1.5; expression > 10 reads per million. Experiments were performed three independent times for siRNA transfection and for RNA extraction. The list of genes obtained by RNA-Seq analysis is provided in Table S1.

Analysis of cell migration

$6x10^5$ T47D cells were plated on 96-well ImageLock plates (Essen BioScience) for 24h at 37°C and then scratched (800 µm width) with the Wound Maker (Essen BioScience). Addition of R5020 or vehicle ethanol were added in the medium just after scratching and wound closure was followed and evaluated with the Incucyte Live-Cell Imaging System and dedicated software (Essen Bioscience). Cell migration was evaluated by monitoring the evolution of the size of wound closure (µm) for 24h maximum, in order to assess the contribution of cell proliferation to gap filling. Since wound width decreases as cell migration progresses over time, we represented the results as graphs indicating the rate of migration, corresponding to the change in wound area over time, extrapolated from three independent experiments, each one performed in triplicate.

Analysis of cell proliferation

$4x10^3$ T47D and $2x10^3$ $T47D_{WT}$ or $T47D_{R637K}$ stable cells were seeded onto a 96-well plate 5h before incubation with the different hormones (E2, R5020 or ethanol). Images were acquired using an IncuCyte ZOOM over 7 days and cell proliferation was measured as the percentage of cell density observed over this period. Results are represented as graphs indicating the rate of proliferation over time, extrapolated from at least three independent experiments, each one performed in triplicate.

Colony formation assay

Cells were seeded into 6-well plates (600 cells/well) and left for 8–12 days until formation of visible colonies. Colonies were washed with PBS and fixed with 10% acetic acid/10% methanol for 20 minutes, then stained with 0.4% crystal violet in 20% ethanol for 20 minutes. After staining, the plates were washed and air-dried, and colony numbers were counted.

Supplemental Tables

Table S2, Related to Methods | Plasmids sequences

Name	Forward sequence (5' – 3')	Reverse sequence (5' – 3')
PR-1	GATATCTGACTGAGCTGAAGGCAAAGG	CTCGAGTTACTGCTCCACCAGGGCGAC
PR-2	GATATCTGGACGCGCCGATGGCGCCC	CTCGAGTTATGGGCTCTGGCTGGCTTC
PR-3	GATATCTGCAATACAGCTTCGAGTCATTACC	CTCGAGTTACTTTTTAAATTTTCGACC
PR-4	GATATCTGTTCAATAAAGTCAGAGTTG	CTCGAGTTATGGTGGAATCAACTG
PR-5	GATATCTGCTGATCAACCTGTTAATGAG	CTCGAGTTACTTTTTATGAAAGAGAAGG
PR-3/ PR-R637A	GCTGGCATGGTCCTTGGAGGTGCAAAATTTAAAAAGTAACTCGAG	CTCGAGTTACTTTTTAAATTTTGCACCTCCAAGGACCATGCCAGC
PR-R637K	CAGGCTGGCATGGTCCTTGGAGGTAAAAAATTTAAAAAGTTCAATAAAGTC	GACTTTATTGAACTTTTTAAATTTTTTACCTCCAAGGACCATGCCAGCCTG

Table S3, Related to Methods | List of antibodies and respective dilutions

PROTEIN NAME	Company	Reference	IB	IP	IF	PLA	ChIP	Species
EGFR	Ozyme (CST)	#4267	1/500e					Rabbit
EGR1	SCBT	Sc-515830	1/500e					Mouse
ERK1/2	CST	#4695	1/2000e					R
GAPDH	SCBT	Sc-4724	1/1000e					M
H3K4me3	Diagenode	C15410003					4µg	R
H4	CST	#13919	1/1000e					R
H4R3me2as	ActiveMotif	#39705	1/500e		1/1000e			R
IgG	CST	#2729		2 µg			4µg	R
Met-R637-PR	Home made		1/100e	15µL	1/300e			R
Pan-methyl-R	CST	#13522	1/500e	4µL		1/1000e		R
p-ERK1/2	CST	#5726	1/2000e					R
p-P38	CST	#9211	1/500e					R
p-PDK1	CST	#3438	1/1000e					R
p-PR	CST	#13736	1/500e					R
PR	SCBT	Sc-7208	1/2000e	2µg			4µg	R
PR	ThermoFischer	MA1-12626	1/1000e		1/500e	1/500e		M
PRMT1	Bethyl Lab.	#A300-722A		2µg			4µg	R
PRMT1	Millipore	#07-404	1/2000e			1/1000e		R
PRMT1	Sigma	P1620	1/500e			1/500e		M
SGK1	SCBT	Sc-28338	1/300e					M
Tubulin α	Sigma	T6074	1/10000e					M
V5-tag	Life Technol.	R920-25	1/1000e					M

Table S4, Related to Methods | Primers sequences

EXPERIMENT	TARGET GENE	Forward sequence (5' – 3')	Reverse sequence (5' – 3')
RT-qPCR	***CCND1***	AAGCTCAAGTGGAACCT	AGGAAGTTGTTGGGGC
	CD44	TTTGCATTGCAGTCAACAGTC	GTTACACCCCAATCTTCATGTCCAC
	EGFR	GACAGGCCACCTCGTCG	CCGGCTCTCCCGATCAATAC
	EGR1	GGCGAGCAGCCCTACGAGC	GTATAGGTGATGGGGGGCAGTC
	IGFBP5	GGTTTGCCTCAACGAAAAGA	CGGTCCTTCTTCACTGCTTC
	IGF1R	TGTCCAGGCCAAAACAGGA	CGGGTTCACAGAGGCATACA
	FKBP5	GGATATACGCCAACATGTTCAA	CCATTGCTTTATTGGCCTCT
	NRDG1	GGCAACCTGCACCTGTTCATCAAT	TGAGGAGAGTGGTCTTTGTTGGGT
	PGR	TGCCTGAAGTTTCGGCCAT	CGCCAACAGAGTGTCCAAGA
	PRMT1	CGCCTCTTGAAGAAGTGTCCT	GATGCCAAAGTGTGCGTAGG
	STAT5A	AAGCCCCACTGGAATGATGG	GGAGTCAAACTTCCAGGCGA
	SGK1	CATAGGAGTTATTGGCAAT	CTTCCATCTCACTAACCA
	28S	CGATCCATCATCCGCAATG	AGCCAAGCTCAGCGCAAC
ChIP-qPCR	***EGFR* +1960**	GAATCTCTGGACTCTGTTCTCAGGTA	CTAGGACTATGTCATTAGCAGATCAG
	***FKBP5* (PRE)**	TAATAGAGGGGCGAGAAGGCAGA	GGTAAGTGGGTGTGCTCGCTCA
	***STAT5A* +6896**	GGACTACTGTGAATTGGCTCGT	GCTTTCTGTTTCTGTTCCTTGA
	hChr1 (NG)	CGGGGGTCTTTTTGGACCTT	GAAACACGGCTGCCAGAAAC

References

Dehairs, J., Talebi, A., Cherifi, Y., and Swinnen, J.V. (2016). CRISP-ID: decoding CRISPR mediated indels by Sanger sequencing. Sci Rep *6*, 28973.

Kastner, P., Krust, A., Turcotte, B., Stropp, U., Tora, L., Gronemeyer, H., and Chambon, P. (1990). Two distinct estrogen-regulated promoters generate transcripts encoding the two functionally different human progesterone receptor forms A and B. EMBO J. *9*, 1603–1614.

Le Romancer, M., Treilleux, I., Leconte, N., Robin-Lespinasse, Y., Sentis, S., Bouchekioua-Bouzaghou, K., Goddard, S., Gobert-Gosse, S., and Corbo, L. (2008). Regulation of estrogen rapid signaling through arginine methylation by PRMT1. Mol. Cell *31*, 212–221.

Robin-Lespinasse, Y., Sentis, S., Kolytcheff, C., Rostan, M.-C., Corbo, L., and Le Romancer, M. (2007). hCAF1, a new regulator of PRMT1-dependent arginine methylation. J. Cell. Sci. *120*, 638–647.

Teyssier, C., Ma, H., Emter, R., Kralli, A., and Stallcup, M.R. (2005). Activation of nuclear receptor coactivator PGC-1alpha by arginine methylation. Genes Dev. *19*, 1466–1473.